ResearchGate

See discussions, stats, and author profiles for this publication at: https://www.researchgate.net/publication/223766752

Geometric characterization and parametric representation of the singularity manifold of a 6–6 Stewart platform manipulator

Article *in* Mechanism and Machine Theory · November 2006

DOI: 10.1016/j.mechmachtheory.2005.12.006

CITATIONS
65

READS
358

2 authors:

Sandipan Bandyopadhyay
Indian Institute of Technology Madras
95 PUBLICATIONS **511** CITATIONS

SEE PROFILE

Ashitava Ghosal
Indian Institute of Science
155 PUBLICATIONS **1,789** CITATIONS

SEE PROFILE

Some of the authors of this publication are also working on these related projects:

Project Resolution of redundancy View project

Project Motor learning project View project

All content following this page was uploaded by Ashitava Ghosal on 31 October 2017.

The user has requested enhancement of the downloaded file.

Geometric characterization and parametric representation of the singularity manifold of a 6-6 Stewart platform manipulator

Sandipan Bandyopadhyay* and Ashitava Ghosal†
Department of Mechanical Engineering
Indian Institute of Science
Bangalore 560 012

Abstract

In this paper, we present a compact closed-form expression for the singularity manifold of a class of 6-6 Stewart platform manipulators most commonly used in research and industry. The singularity manifold is obtained as the hyper-surface in the task-space, $SE(3)$, on which the wrench transformation matrix for the top platform degenerates. This condition leads to an extremely large expression containing algebraic and trigonometric functions of the architecture, position and orientation variables. We present algorithms for efficient symbolic simplification of such large expressions. Using these algorithms, for a given *architecture and orientation*, the singularity manifold is obtained as a cubic surface in $\Re^3$. The symbolic computations yield a simple parametric expression for the surface in terms of the architectural and orientation parameters of the manipulator, and allows us to *completely* characterise and visualise the singularity manifold. We show that, in general, the cubic surface is a one-parameter family of hyperbolas in planes parallel to the base of the manipulator. It is further shown that the hyperbola degenerates to a parabola in a unique plane, and to a pair of straight lines in four other planes. The explicit parameterization allows us to obtain the location of each of these special planes analytically. For a given *architecture and position*, the singularity manifold is a surface in $SO(3)$, which can be, in general, algebraically described by a 6th degree polynomial in the Rodrigue's parameters. In this paper, we present explicit expressions for the polynomial defining the orientation singularity manifold in terms architecture and orientation parameters. The theoretical results are illustrated with several numerical examples.

1 Introduction

In parallel manipulators, singularities lead to loss of rigidity in certain direction(s), and unbounded loads at one or more passive joints. Therefore identification and avoidance of singularities in such

*The author is presently with the General Motors India Science Laboratory, Bangalore. e-mail: sandipan.bandyopadhyay@gm.com

†Corresponding author. e-mail: asitava@mecheng.iisc.ernet.in

manipulators are issues of practical importance, and they have attracted a significant volume of research. However, due to the inherent complexity of the parallel kinematic structures, analysis of their singularities is particularly difficult. Closed form results are hard to come by, and geometric characterisation of the singularity manifold is generally restricted to relatively simple manipulators, such as the 3-DOF planar parallel manipulator [21] or 3-DOF spatial parallel manipulator [1, 8]. Singular configurations of the Stewart platform manipulators (SPMs) have been studied by different researchers using various techniques, such as screw geometry, line geometry, and computational algebra. Hunt [11] describes one of the earliest known singular configurations of a 3-3 SPM using screw theory. The result of Fichter [4] also concerns the 3-3 SPM, and SPMs with semi-regular platforms (SRSPMs). Merlet [16, 17] has used Grassmann geometry to study a greater variety of SPM architectures, and has presented a comprehensive treatment of singularities of 3-3 and 6-3 classes of SPMs. However, due to the complexity of the more general 6-6 SPM's, the same formalism has not been applied to these manipulators [17].

Determination of the singularity manifold of the 6-6 SPMs is an active area of research, and in recent times, researchers have used various computational algebra tools to arrive at the analytical form of the same. St-Onge and Gosselin [22] have used the singularity condition proposed in [6], and derived a polynomial expression for the singularity manifold of the general SPM. Kim and Chung [12] have used an alternate formulation of the linear velocity relationships to arrive at a similar expression with lesser number of terms. St-Onge and Gosselin [23] have refined their earlier work to report the algebraic structure of the singularity manifold of the SPM for various architectural classes. The analytical expressions have been derived in terms of sums of determinants of 6×6 symbolic matrices, and the degree of the minimal polynomial expression representing the singularity locus has been presented for various SPM architectures. It is mentioned, for example, that a SPM with semi-regular hexagon has a cubic singularity locus with the degree of the position variables, x, y, z as 2, 2 and 3, respectively, and the polynomial has 16 non-zero coefficients resulting from 48 non-vanishing determinants. However, the coefficients of the cubic have not been explicitly obtained, and the dependence of the singularity manifold on the architectural and pose parameters is very difficult to obtain from the formulation. Further, in St-Onge and Gosselin [23], the visualisation of the singularity manifold is through a CAD software and an explicit parameterization of the singularity manifold would be far superior. Di Gregorio [7, 9] has proposed a method, based on expansion of ten 3×3 determinants, to obtain the singularity locus, and he has mentioned that the singularity locus is of degree 3 in terms of position variables and degree 6 in terms of Rodrigue's parameters. However, in this case too the explicit expressions for the singularity locus have not been presented.

In the above mentioned body of literature, the visualisation of the 5-dimensional singularity manifold has been done mostly in terms of its 3-dimensional projection on $\Re^3$, i.e., the positional subspace of $SE(3)$. Li et al.[13] present analytical expression of the singularity locus in terms of x, y, z and three Euler angles. They report that the singularity locus can be at most cubic in sine and cosine of the Euler angles and they present in a numerical example the plot of the singularity locus in terms of the tangent half-angle of the three Euler angles when $x = y = z = 0$. It is, however, not clear if the degree of six, in terms of tangent half-angles, is applicable to any arbitrary position.

This paper presents compact, explicit solutions to the above mentioned problems for an SRSPM. From the condition of the degeneracy of the wrench transformation matrix of the top platform, we obtain an analytical expression defining a 5-dimensional manifold in $SE(3)$, in terms of the architectural, position, and orientation parameters. For a given *architecture and orientation* of the

top platform, the singularity manifold $\mathcal{M} \in SE(3)$[1] reduces to the singularity surface $\mathcal{S}_{\boldsymbol{p}} \in \Re^3$. The surface $\mathcal{S}_{\boldsymbol{p}}$ is cubic in z, and quadratic in x, y where $\boldsymbol{p}(x, y, z)$ represents the center of the top platform in a global reference frame, and thus the degree of the singularity locus is consistent with those reported in [12, 23, 7, 9]. We, however, further show that $\mathcal{S}_{\boldsymbol{p}}$ intersects planes parallel to the base of the manipulator in a one-parameter family of hyperbolas except for a unique plane, where the intersection is a parabola. In addition, there are 4 planes in which the hyperbolas degenerate into a pair of straight lines. This geometric characterisation leads to an explicit parametric description of $\mathcal{S}_{\boldsymbol{p}}$, aiding easy visualization and further study of its properties. For a given *architecture and position*, the singularity manifold reduces to a surface $\mathcal{S}_{\mathcal{O}} \in SO(3)$, which is of 6th degree in the Rodrigue's parameters, and gives the orientation singularities at any point $\boldsymbol{p}(x, y, z)$. The degree of the singularity locus is again consistent with those mentioned in [9, 13], and we present explicit closed-form expressions for the polynomial defining $\mathcal{S}_{\mathcal{O}}$. The two surfaces, $\mathcal{S}_{\boldsymbol{p}}$ and $\mathcal{S}_{\mathcal{O}}$ present complimentary descriptions of the singularity manifold $\mathcal{M}$ of the SRSPM. The closed-form expressions in a simple and compact form and the geometric characterization of $\mathcal{S}_{\boldsymbol{p}}$ are the main contributions of this paper. These analytical results are expected to make the important task of path planning, singularity avoidance and design easier.

The initial analytical expression obtained from the condition of the degeneracy of the wrench transformation matrix contains a very large number of terms involving trigonometric and algebraic functions of the position, orientation and architectural variables, and special symbolic computation and simplification algorithms have been developed and used to reduce the analytic expression to the compact form mentioned above. The algorithms developed for symbolic computations are not limited to singularity analysis of a SRSPM alone and can be used for a variety of parallel manipulators and multi-body systems, and hence they embody another important contribution of this paper.

The theory and algorithms developed in this paper relies only on a certain structure of the wrench transformation matrix, and is therefore applicable to a wide variety of spatial parallel manipulators, including all forms of the SPM, such as 3-3, 3-6, 6-3, 6-6, with regular, irregular, planar, or non-planar top and bottom platforms. In this paper, we have chosen the 6-6 SRSPM to illustrate the theory and algorithms developed as this is the most common architecture of SPMs used in numerous applications, such as the flight simulators, tank cabin simulator, radio-telescope pointing device etc. (for a more detailed and interesting list of applications, refer to [17]). The paper is organized as follows: in section 2, we present the kinematic modeling of the Stewart platform manipulator and the SRSPM. In section 3, we present the algorithms for symbolic computations and simplification of expressions containing algebraic and trigonometric terms. In section 4, we present the analytical expressions for the singularity manifolds of SRPSM. In section 5, we present several numerical examples illustrating the theory developed in this paper, and finally, we present the conclusions and scope for future work in section 6.

[1] In this paper, we use the standard terms $SE(3)$ to denote the space of rigid-body motion, $se(3)$ to denote the space of twists, $SO(3)$ to denote the space of orientations, and $se^*(3)$ to denote the space of wrenches (for details, see for e.g., [19]).

2 Kinematic modeling of a Stewart platform manipulator

In this section, we describe the geometry of the Stewart platform manipulator, and present a kinematic model of the same for the purpose of singularity computations. From the general kinematic equation for singularity, we obtain the singularity condition for the special case of a SRSPM.

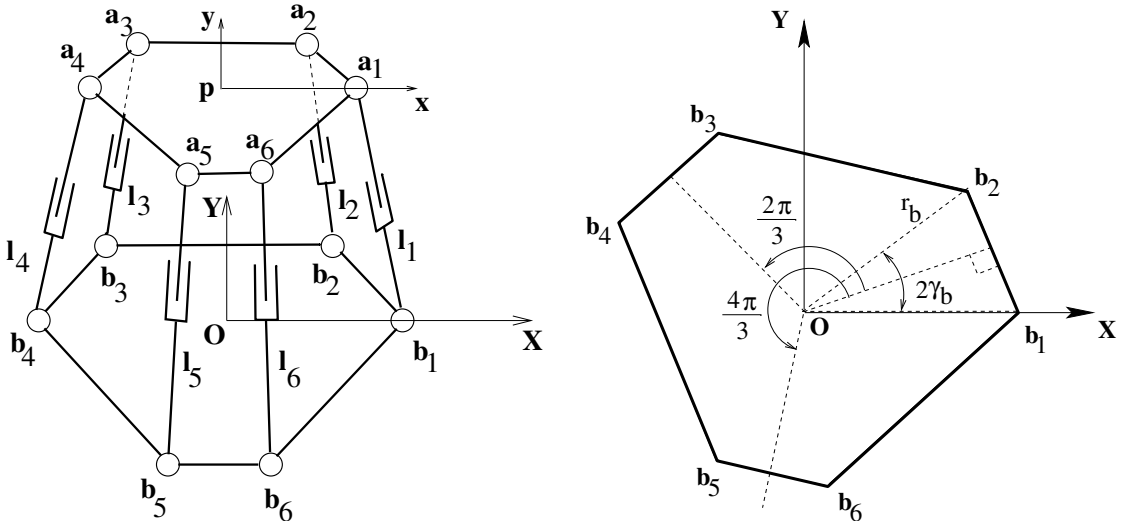

(a) The manipulator

(b) Bottom platform

Figure 1: Geometry of the Stewart platform manipulator

2.1 Formulation of singularity in the task space

We derive the singularity condition of the Stewart platform in terms of the *task-space* coordinates, i.e., using a parameterization of $SE(3)$. We denote the position of the centre of the top platform, the point $\boldsymbol{p}$, by the vector $(x, y, z)^T$, and the orientation of the top platform by $\boldsymbol{R} \in SO(3)$. The loop-closure equations can be written as

$$\boldsymbol{p} + \boldsymbol{R}\boldsymbol{a}_i - \boldsymbol{b}_i - l_i\boldsymbol{s}_i = \boldsymbol{0} \qquad i = 1, ..., 6 \tag{1}$$

where l_i denotes the length of the ith leg and $\boldsymbol{a}_i, \boldsymbol{b}_i$ locate the leg connection points with respect to the platform centers in respective frames (see figure 1(a)), and $\boldsymbol{s}_i$ denotes the ith screw axis along the respective leg. The screw axis can be written in terms of the Cartesian, and actuated variables as

$$\boldsymbol{s}_i = \frac{1}{l_i}(\boldsymbol{p} + \boldsymbol{R}\boldsymbol{a}_i - \boldsymbol{b}_i) \tag{2}$$

Denoting the actuation force along the ith leg as f_i, the wrench imparted on the top platform may be expressed in the base reference frame as

$$\boldsymbol{W}_i = (f_i\boldsymbol{s}_i; (\boldsymbol{R}\boldsymbol{a}_i) \times f_i\boldsymbol{s}_i) \tag{3}$$

Using the expression for $\boldsymbol{s}_i$ from equation (2), $\boldsymbol{W}_i$ may be written as

$$\boldsymbol{W}_i = \left(\frac{f_i}{l_i}(\boldsymbol{p} + \boldsymbol{R}\boldsymbol{a}_i - \boldsymbol{b}_i); \frac{f_i}{l_i}((\boldsymbol{R}\boldsymbol{a}_i) \times (\boldsymbol{p} - \boldsymbol{b}_i)) \right) \tag{4}$$

Denoting the force and moment parts of the resultant wrench applied on the top platform due to all the leg forces as $\boldsymbol{W} = \sum_{i=1}^{6} \boldsymbol{W}_i = (\boldsymbol{F};\boldsymbol{M})$, the equation for statics of the top platform may be written as

$$\begin{pmatrix} \frac{1}{l_1}(\boldsymbol{p} + \boldsymbol{R}\boldsymbol{a}_1 - \boldsymbol{b}_1)_1 & \dots & \frac{1}{l_6}(\boldsymbol{p} + \boldsymbol{R}\boldsymbol{a}_6 - \boldsymbol{b}_6)_1 \\ \frac{1}{l_1}(\boldsymbol{p} + \boldsymbol{R}\boldsymbol{a}_1 - \boldsymbol{b}_1)_2 & \dots & \frac{1}{l_6}(\boldsymbol{p} + \boldsymbol{R}\boldsymbol{a}_6 - \boldsymbol{b}_6)_2 \\ \frac{1}{l_1}(\boldsymbol{p} + \boldsymbol{R}\boldsymbol{a}_1 - \boldsymbol{b}_1)_3 & \dots & \frac{1}{l_6}(\boldsymbol{p} + \boldsymbol{R}\boldsymbol{a}_6 - \boldsymbol{b}_6)_3 \\ \frac{1}{l_1}((\boldsymbol{R}\boldsymbol{a}_1) \times (\boldsymbol{p} - \boldsymbol{b}_1))_1 & \dots & \frac{1}{l_6}((\boldsymbol{R}\boldsymbol{a}_6) \times (\boldsymbol{p} - \boldsymbol{b}_6))_1 \\ \frac{1}{l_1}((\boldsymbol{R}\boldsymbol{a}_1) \times (\boldsymbol{p} - \boldsymbol{b}_1))_2 & \dots & \frac{1}{l_6}((\boldsymbol{R}\boldsymbol{a}_6) \times (\boldsymbol{p} - \boldsymbol{b}_6))_2 \\ \frac{1}{l_1}((\boldsymbol{R}\boldsymbol{a}_1) \times (\boldsymbol{p} - \boldsymbol{b}_1))_3 & \dots & \frac{1}{l_6}((\boldsymbol{R}\boldsymbol{a}_6) \times (\boldsymbol{p} - \boldsymbol{b}_6))_3 \end{pmatrix} \begin{pmatrix} f_1 \\ f_2 \\ f_3 \\ f_4 \\ f_5 \\ f_6 \end{pmatrix} = \begin{pmatrix} \boldsymbol{F} \\ \boldsymbol{M} \end{pmatrix} \tag{5}$$

Equation (5) can be written compactly as

$$\boldsymbol{W} = \boldsymbol{H}\boldsymbol{\tau} \tag{6}$$

where $\boldsymbol{\tau} = (f_1, f_2, f_3, f_4, f_5, f_6)^T$ is the generalized leg force vector, and the 6×6 matrix on the left hand side of the equation is the wrench transformation matrix of the top platform, $\boldsymbol{H}$. It may be noted that the use of equation (2) ensures that equation (6) is kinematically consistent, namely the loop closure equations are satisfied.

The wrenches lie in the column space of $\boldsymbol{H}$ for all joint forces $\boldsymbol{\tau}$. For a fully actuated non-redundant 6-degrees-of-freedom spatial manipulator, $\boldsymbol{H}$ is a 6×6 matrix, and in a general configuration, it is invertible. The column space of $\boldsymbol{H}$ spans $se^*(3)$ in such a case, i.e., all the possible wrenches $\boldsymbol{W}$ at the end-effector can be supported by the joint force vector. However, if there exists a wrench of finite magnitude in $se^*(3)$ that can not be supported by a *finite* joint force vector $\boldsymbol{\tau}$, then the left-nullspace of $\boldsymbol{H}$, i.e., the orthogonal complement of the column space of $\boldsymbol{H}$ with respect to $se^*(3)$ is non-null, and $\boldsymbol{W}$ lies in that space. This implies that

$$D_{\boldsymbol{H}} = \det(\boldsymbol{H}) = 0 \tag{7}$$

The singularity manifold $\mathcal{M}$ is defined by the equation (7). Further, from equation (5), $D_{\boldsymbol{H}}$ may be written as

$$D_{\boldsymbol{H}} = \frac{1}{l_1 l_2 l_3 l_4 l_5 l_6} \det \begin{pmatrix} (\boldsymbol{p} + \boldsymbol{R}\boldsymbol{a}_1 - \boldsymbol{b}_1)^T & \dots & (\boldsymbol{p} + \boldsymbol{R}\boldsymbol{a}_6 - \boldsymbol{b}_6)^T \\ ((\boldsymbol{R}\boldsymbol{a}_1) \times (\boldsymbol{p} - \boldsymbol{b}_1))^T & \dots & ((\boldsymbol{R}\boldsymbol{a}_6) \times (\boldsymbol{p} - \boldsymbol{b}_6))^T \end{pmatrix} \tag{8}$$

and, $\mathcal{M}$, as defined in equation (7) is clearly independent of l_i. Hence, the singularity condition can be restated as

$$\det(\boldsymbol{H}_1) = \det \begin{pmatrix} (\boldsymbol{p} + \boldsymbol{R}\boldsymbol{a}_1 - \boldsymbol{b}_1)^T & \dots & (\boldsymbol{p} + \boldsymbol{R}\boldsymbol{a}_6 - \boldsymbol{b}_6)^T \\ ((\boldsymbol{R}\boldsymbol{a}_1) \times (\boldsymbol{p} - \boldsymbol{b}_1))^T & \dots & ((\boldsymbol{R}\boldsymbol{a}_6) \times (\boldsymbol{p} - \boldsymbol{b}_6))^T \end{pmatrix} = 0 \tag{9}$$

where $\boldsymbol{H}_1$ is the 6×6 matrix on the right-hand side of the above equation.

It may be noted that this form is true for all SPMs, and similar spatial parallel manipulators, whose wrench transformation matrix is of the form of equation (5). The singularity condition for a SPM, equation (9), can be further simplified for a SRSPM by a suitable choice of a coordinate system and a parameterization of $SO(3)$ and this is discussed next.

2.2 Geometry of the SRSPM

The SRSPM has hexagonal top and bottom platforms, with alternate sides in each platform having identical length. There is a 3-way symmetry in each platform, and the adjacent pairs of legs are arranged symmetrically about the three radial lines of symmetry in each platform. The angular spacings between the adjacent pairs of legs are denoted by $2\gamma_t$, and $2\gamma_b$ for the top and bottom platforms respectively. Without any loss of generality, the circum-radius of the bottom platform is scaled to unity[2] and thereby one architectural parameter is eliminated from all subsequent computations. The top circum-radius is denoted by r_t.

In literature, it is a *de facto* convention to choose one of the three axes of symmetry in the platforms as the local X direction. Therefore, the angular spacing of the legs (in the top platform for instance) become $\boldsymbol{\gamma}_t = (-\gamma_t, \gamma_t, 2\pi/3 - \gamma_t, 2\pi/3 + \gamma_t, 4\pi/3 - \gamma_t, 4\pi/3 + \gamma_t)$ with respect to the corresponding X axis. However, we choose the X axis to pass through the connection point of the first leg in each platform, such that the spacings are given by $\boldsymbol{\gamma}_t = (0, 2\gamma_t, 2\pi/3, 2\pi/3 + 2\gamma_t, 4\pi/3, 4\pi/3 + 2\gamma_t)$, $\boldsymbol{\gamma}_b = (0, 2\gamma_b, 2\pi/3, 2\pi/3 + 2\gamma_b, 4\pi/3, 4\pi/3 + 2\gamma_b)$ respectively in the top and bottom platform. In this way, three of the leg connection points lie on the axes of symmetry, and the arrangement results in a significant reduction of complexity in all subsequent computations. The manipulator along with the frames of reference used is shown in figure 1(a), and the bottom platform, in figure 1(b).

With the above choice of the coordinate system, the SRSPM is described by 9 parameters: $(r_t, \gamma_b, \gamma_t)$ defining the architecture, and 6 local coordinates of $SE(3)$ - as seen later an algebraic representation of the rotation matrix is chosen using the *Rodrigue's parameters* $\boldsymbol{c} = (c_1, c_2, c_3)$ (see Appendix A for details) as this helps in symbolic computations. Therefore, the singularity manifold, $\mathcal{M}$, can be described by a hyper-surface in $\Re^9$, each point of which defines one singular configuration[3].

3 Simplification of algebraic-trigonometric expressions and their canonical forms

In kinematic computations and in attempts to obtain closed form analytic expressions, we frequently come across *large* and *complex* mathematical expressions involving algebraic and trigonometric terms. The symbolic simplification of large and complex expressions is an old problem and is known to be NP hard and the use of a computer algebra system (CAS) is necessary to simplify and manipulate such expressions. In this section, we describe a scheme for this purpose using three *canonical* forms of such expressions. We have used the scheme in conjuction with `Mathematica`[24] in our work to obtain compact, closed form, analytic expressions for the singularity manifold, $\mathcal{M}$, of a Stewart platform manipulator.

[2]We use *radians* for the angular unit, while the length unit for base platform can be chosen as convenient. All other lengths are non-dimensionalized.

[3]It may be noted that the 9 variables determine l_i's via the inverse kinematics relationships and hence l_i's themselves do not influence the dimension of the $\mathcal{M}$.

3.1 Complexity of a symbolic expression and limitations of heuristic simplification schemes

The notion of complexity of an expression, in the domain of symbolic computation, tend to be case-specific, and therefore non-unique. Likewise, the definition of the *most simplified* or *canonical* form of an expression is also subjective. Various practical (albeit heuristic) measures of complexity are used in CAS's to detect possibilities of automatic simplification. One common practice is to construct the *tree* description of the expression, and use the total number of leaves or terminal nodes as a measure of complexity (e.g., the default measure used in the simplification schemes of the CAS `Mathematica`). The heuristic measures do not necessarily make use of the algebraic structure of the expression, and are not proof against missing out certain non-trivial simplifications. Apart from this theoretical limitation, the practical difficulties of such simplification schemes can be forbidding. We discuss the most outstanding issues below.

- For any large and complex expression, such as $\det(\boldsymbol{H}_1) = 0$, the simplification algorithms take very long time and quickly use up all the computer memory. In the context of `Mathematica`, `FullSimplify` quickly runs out of memory and one has to compromise by using the more rudimentary `Simplify`. However, `Simplify` does not simplify *completely*, and we are left with still complex descriptions of the actual expression. Due to the incomplete simplification of the coefficients of a polynomial, some of the actually zero coefficients may not be identified as zeros. This would give wrong information about the degree of the polynomial if it happens so with the leading coefficient, or report a wrong algebraic structure in general.

- It is known that a general univariate polynomial having degree greater than 4 can only be solved numerically (see, for example, [10]), and that the zeros of a polynomial can be sensitive to the errors in the coefficients, particularly if the degree of the polynomial is high [20]. Due to accumulation of errors in the lengthy numerical evaluation of the incompletely simplified coefficients, numerically obtained zeros of a high degree polynomial can be significantly erroneous. Further, the actual zeros which escape identification, can show up as *small* non-zero values, and corrupt the accuracy all subsequent computations. Although it is possible to increase the numerical precision of the evaluation process almost arbitrarily within a CAS, it can only be done at the cost of greater computational time, and inflexibility of implementation.

To overcome the problems associated with heuristic simplification schemes, we develop a *deterministic* substitute for a class of expressions involving both trigonometric and algebraic terms. The end result of these schemes in each case is a *canonical form* of the input expression.

3.2 Deterministic simplification schemes using canonical forms of expressions

Let E be a symbolic expression involving m algebraic variables $\boldsymbol{x} = (x_1, x_2, \ldots, x_m)$, and l trigonometric variables $\boldsymbol{\gamma} = (\gamma_1, \gamma_2, \ldots, \gamma_l)$ with the property that it can be cast as a polynomial in *at least* one of the variables[4]. Without loss of generality, we choose the lexicographical variable order (i.e., $x_1 \succ x_2 \succ \cdots \succ x_m$) for our discussion (see, for example, [3]).

[4]In the case of absence of any such variable, we have to use only trigonometric simplifications.

It is known in literature that multivariate polynomials over various coefficient domains, such as $\Re, \mathbb{C}, \mathbb{Q}$, can have several canonical representations, such as the *nested canonical form* and the *monomial-based canonical form* (see [5, 2] for various representations of multivariate polynomials). We propose to generalize the ideas behind these representations to the case where the coefficients are complicated expressions of trigonometric variables, and employ these concepts for simplification of complex expressions. Apart from the above two forms, we use a combination of the these, and term it the *hybrid canonical form*. The common features of all three schemes are:

- Isolation of algebraic and trigonometric variables using the algebraic structure of the expression.
- Decomposition of the original expression into number of smaller terms.
- Grouping and simplification of the trigonometric subexpressions.
- Reconstruction of the original expression from simplified subexpressions.

In the following, we discuss these three forms, their merits and demerits.

3.2.1 Simplification using the nested canonical form

We explain the scheme for the case of univariate polynomials, and then generalize it to the multivariate case. Let E be a degree n^1 polynomial in x_1 represented as

$$E = \sum_{i=0}^{n^1} C_i^1 x_1^{n^1-i} = \boldsymbol{C}^1 \cdot \boldsymbol{p}^1 \tag{10}$$

where the *power vector* $\boldsymbol{p}^1$ consists of the powers of x_1: $\boldsymbol{p}^1 = (x_1^{n^1}, x_1^{n^1-1}, \ldots, x_1, 1)$ and the *coefficient vector* $\boldsymbol{C}^1 = (C_0^1, C_1^1, \ldots, C_{n^1-1}^1, C_{n^1}^1)$ contains the corresponding coefficients. Note that in such a description, all the trigonometric terms appear only in the elements of the coefficient vector $\boldsymbol{C}^1$. The major consequence of this step is that the original expression is broken into (n^1+1) separate terms, algebraic complexities of each of which are lesser than that of E due to the absence of the variable x_1. In spite of the fact that (n^1+1) expressions have to be simplified now, the computational cost of simplifying $\boldsymbol{C}^1$ is lesser and the final results better than simplifying E directly [2]. The simplification scheme for E may be written as

$$simplify(E) = \sum_{i=0}^{n^1+1} Simplify(\boldsymbol{C}_i^1)\boldsymbol{p}_i^1 = Simplify(\boldsymbol{C}^1).\boldsymbol{p}^1 \tag{11}$$

where *simplify* denotes our scheme of simplification, and *Simplify* denotes the simplification operator of the CAS employed. It may be noted that the coefficients can be simplified sequentially, or in parallel, as the case may be, and then put together to reproduce the original expression in a simplified form.

The gains in speed and compactness become significantly more prominent with the increase in *depth* of transformation of type (10), i.e., with more number of algebraic variables. We treat each

of C_i^1 as our input expression now, and repeat the same procedure as above in a recursive manner. Using the above notation, we can write

$$C_i^1 = \sum_{j=0}^{n_i^2} C_{ij}^2 x_2^{n_i^2-j} = \boldsymbol{C}_i^2 \cdot \boldsymbol{p}_i^2 \tag{12}$$

where $\boldsymbol{p}_i^2 = (x_2^{n_i^2}, x_2^{n_i^2-1}, \ldots, x_2, 1)$ and $\boldsymbol{C}_i^2 = (\boldsymbol{C}_{i0}^2, \boldsymbol{C}_{i1}^2, \ldots, \boldsymbol{C}_{n_i^2-1}^2, \boldsymbol{C}_{n_i^2}^2)$ is the corresponding coefficient vector, which is free of x_1, x_2. The integer n_i^2 denotes the degree of C_i^1 in x_2. At this stage, the simplified form of E would be given as

$$simplify(E) = \left(\sum_{j=0}^{n^1} Simplify\left(\boldsymbol{C}_j^2\right) \cdot \boldsymbol{p}_j^2 \right) \cdot \boldsymbol{p}^1 \tag{13}$$

A comparison of equations(11, 13) illustrates how the operator $Simplify$ penetrates deeper into the expressions down the coefficient tree with each algebraic variable isolated. It is important to note that all simplifications are done *only at the leaves of the coefficient tree.* As a result, individual calls to the simplification routine deal with progressively smaller, and simpler expressions as we move down the tree, and yield much faster, better results than can be obtained at the higher levels of the tree with comparable computational cost.

The process can be continued recursively, resulting in the set of vectors $\boldsymbol{C}_{ij}^3$ at the next level, up to $\boldsymbol{C}_{i_1 i_2 \ldots i_{m-1}}^m$ at the final level. These final vectors are independent of $\boldsymbol{x}$, and contain the trigonometric terms in $\boldsymbol{\gamma}$. The coefficients of the lowest level are now subjected to the deterministic trigonometric transformations and the corresponding simplifications obtained with remarkable gain in speed and compactness. The algorithm can now trace back via compositions of the form of equation (13), and return the final simplified expression.

As an example of nested canonical form of expressions, we cast the singularity polynomial of equation (20) of section 4.2 in this form:

$$\begin{aligned} E =& x^2(E_1 z + E_2) + x(y(E_3 z + E_4) + E_5 z^2 + E_6 z + E_7) + y^2(E_8 z + E_9) + \\ & y(E_{10} z^2 + E_{11} z + E_{12}) + E_{13} z^3 + E_{14} z^2 + E_{15} z + E_{16} \end{aligned} \tag{14}$$

We observe that the above scheme of simplification has several advantages:

- There is a great increase of speed in the simplification process. Depending on the particular structure of E, an increase of 10 to 100 times was observed in our computations.

- The final expression is obtained in a *canonical form.* From the description of the scheme above, it is apparent that we have traversed the coefficient tree for a multivariate polynomial (which is unique up to the choice of variable order) down to the leaves. The set of leaves, however, depend only on the power-products of x_i's present in E, and is therefore unique for each expression. The leaves may consist of only algebraic expressions in constants from $\Re, \mathbb{C}, \mathbb{Q}$ etc., and trigonometric functions of γ_i. We can first expand these expressions algebraically, and then apply simplifying trigonometric transformations. Both of these steps are *deterministic* in nature, and produce unique results for a given set of simplifying transformations. Therefore the final expression obtained in this process is *not* subjected to any heuristic treatment at any stage, and has a deterministic structure. We call the multivariate polynomial with simplified trigonometric coefficients as the *nested canonical form* of E.

- The returned expression is *free* of expressional redundancies at least as far as trigonometric terms are concerned. In a heuristic simplification scheme, such as minimization of leaf-count of the expression tree, the algebraic structure of the expression is not taken into consideration. Many trigonometric cancellations and/or simplifications may be overlooked as the terms concerned appear at different nodes of the expression tree, and expanding the tree, at least on the onset, can be unfavorable in terms of leaf count. Even the final canonical expression need not be the *best* in terms of leaf-count. However, the trigonometric terms that belong to a particular monomial, and can therefore potentially combine according to trigonometric rules, are brought together under the same node by our scheme. It is therefore guaranteed that *all* possible simplification steps are attempted for a given set of trigonometric transformations available.

- The algebraic structure information (e.g., power products of all the elements of $\boldsymbol{x}$, or any subset thereof), can be obtained trivially from the canonical form. Further algebraic manipulations using the simplified expressions are greatly facilitated due to their standard form.

- One great advantage for algebraic geometry computation with the canonical form is that due to exhaustive simplification of the coefficients, it is possible to identify the zeros among them, if any. Due to the complexity of the expressions, the zeros may not be apparent, and are easy to miss in a heuristic simplification scheme.

There are some disadvantages in using the nested form as the final expression. In general, in a multivariate polynomial, all possible power products are not present. In fact, with increasing number of variables, the number of *missing* power-products is expected to increase rapidly, as all the children of a node corresponding to a missing power at any level can only be zeros. Since many of these zeros can only be identified at the leaves, we can end up with a lot of redundant zeros among them. Further, the same expression can have different coefficient trees if the variable order is changed. Some of the orders can produce better results than the others for the same expression, and the choice of the *best* order is again heuristic. Primarily to overcome these problems, we study another standard form, known as the *monomial-based canonical form*.

3.2.2 Simplification using the monomial-based canonical form

In this representation, we retain the non-zero coefficients of individual power-products in explicit form, and express the polynomial as a sum of monomials in x_i's. At different levels, the expression E can be written as

$$E = \boldsymbol{D}^1 \cdot \boldsymbol{q}^1 = \boldsymbol{D}^2 \cdot \boldsymbol{q}^2 = \cdots = \boldsymbol{D}^m \cdot \boldsymbol{q}^m \tag{15}$$

The vector $\boldsymbol{q}^j$ consists of power-products of $x_1, x_2, \ldots, x_j$ including unity, and the vector $\boldsymbol{D}^j$ consists of the corresponding coefficients. The simplification is done at the lowest level, and the simplification scheme can be written in analogy with equation (11) as

$$simplify(E) = Simplify(\boldsymbol{D}^m) \cdot \boldsymbol{q}^m \tag{16}$$

To construct such a description, we follow the same steps as in the nested canonical form, starting with a variable order. For the case of a single variable x_1, the results are also exactly the same. For

the multivariate case, we construct the coefficient and power arrays in the same way as in equation (10). However, before moving to the next level, we eliminate the zero coefficients from $\boldsymbol{C}^1$. Let the new coefficient vector be $\boldsymbol{C}^{1'}$, and let its size be m^1. We modify the power vector $\boldsymbol{p}^1$ accordingly, and call it $\boldsymbol{p}^{1'}$. The coefficients of the next level can be constructed similarly as

$$C_i^{1'} = \boldsymbol{C}_i^{2'} \cdot \boldsymbol{p}_i^{2'} \tag{17}$$

Now, we construct the array of all power products of x_1, x_2 by taking the union of the arrays $p_i' \boldsymbol{p}_i^{2'}$:

$$\boldsymbol{q}^2 = \bigcup_{i=0}^{m^1} p_i' \boldsymbol{p}_i^{2'} \tag{18}$$

The corresponding array of coefficients, $\boldsymbol{D}^2$, can be constructed similarly, and the process can repeat $(m-1)$ times to give the final arrays of power products $\boldsymbol{q}^m$ and coefficients $\boldsymbol{D}^m$ respectively. The elements of $\boldsymbol{D}^m$ correspond to $\boldsymbol{C}^m_{i_1 i_2 \ldots i_{m-1}}$, and are independent of $\boldsymbol{x}$, and contains all the trigonometric terms which can be simplified in a similar fashion. In fact, given one canonical form, it is not difficult to construct the other. However, this form offers some important advantages:

- Compactness of representation and ease of manipulation: We maintain the coefficients and the powers-products in two vectors explicitly after eliminating all missing terms. Therefore the representation is more compact and easy to maintain and manipulate than the previous one.

- Uniqueness of representation: Given a set of variables, the final vectors $\boldsymbol{D}^m$ and $\boldsymbol{q}^m$ are invariants as sets, and a change of variable order can only reorder them.

- Identification of trivial zeros of an equation: If we have an equation of the form $E = 0$, by converting it to the monomial-based canonical form $E = \boldsymbol{D}^m \cdot \boldsymbol{q}^m$, we get all the power-products in the array $\boldsymbol{q}^m$. It is trivial to obtain the GCD of these power-products, which corresponds to the trivial zeros of the equation. Canceling off the GCD from $\boldsymbol{q}^m$, these trivial zeros can be eliminated, resulting in an equation of lower degree.

- Identification of special structures of an equation: It is possible for the power-products to show certain special patterns, which can be identified trivially from the array $\boldsymbol{q}^m$. For example, in many cases of kinematic analysis, there is symmetry of even order associated with a certain variable, causing the variable to occur only in even powers in $\boldsymbol{q}^m$. Therefore, the square (or some higher even power) of the variable can be replaced by another symbol, reducing the degree of the resulting equation to half (or lesser) of the original.

An example of an expression cast in this form is the left-hand side of equation (20), where the algebraic variables are x, y, z.

The disadvantage of the second canonical form of E becomes apparent with increasing number of algebraic variables, as the array $\boldsymbol{q}^m$ starts growing in size. It is difficult to anticipate *a priori* the actual size of these arrays, as the algebraic structure of E is not known in general. Therefore one can always obtain the monomial-based canonical form as a starting point of simplification. If the arrays are found to be unacceptably large in size, we can arrive at a compromise between ease of operation and size by introducing another form of great practical value: the *hybrid canonical form*, which is discussed next.

3.2.3 Simplification using the hybrid canonical form

The hybrid form makes use of both the nested and the monomial-based canonical forms. In this case, we divide the algebraic variables $\boldsymbol{x}$ into two groups, namely *primary algebraic variables*, and *secondary algebraic variables*. The final expression is returned in the monomial-based form in the primary algebraic variables, while the individual coefficients are put into the nested canonical form. As an example, we write below the hybrid canonical form of the polynomial in equation (20), where x, y are the primary variables, and z alone is the secondary variable:

$$\begin{aligned} E =& x^2(E_1 z + E_2) + xy(E_3 z + E_4) + y^2(E_8 z + E_9) + x(E_5 z^2 + E_6 z + E_7) + \\ &+ y(E_{10} z^2 + E_{11} z + E_{12}) + E_{13} z^3 + E_{14} z^2 + E_{15} z + E_{16} \end{aligned} \tag{19}$$

The advantages of this canonical form are the following:

- By choosing the primary variables as the ones which are expected to be involved in further symbolic computations (such as elimination), we get the corresponding power-products in explicit form, thereby making algebraic manipulations particularly simple.
- The secondary variables are often the ones that are to be evaluated, rather than manipulated symbolically, and subsequently merged numerically into the coefficients of the power-products of the primary variables.
- For relatively large-sized problems, it appears much easier to look into the one sub-problem at a time, e.g., the effect of one variable on the zeros of a polynomial. The partitioning scheme of the hybrid form allows for such focused analysis (see the derivations of $\mathcal{S}_{\boldsymbol{p}}$ and $\mathcal{S}_{\mathcal{O}}$ in the next section for such examples).

For relatively large-scale problems, the hybrid canonical forms turn out to be the most suitable, and we use them extensively in this paper. We also note that after applying one or more of the above simplifications, the expression E can always be subjected to the standard simplification schemes based on number of leaves minimization. It is our observation that such *post-processing* steps can improve the compactness of the final expression as these steps can take advantage of the highly structured canonical forms.

In the next section, we apply these schemes to simplify the singularity condition of the SRSPM, and reduce it to a form amenable to further analysis.

4 Singularity manifold of the SRSPM

In this section, we describe the derivation of the singularity manifold ($\mathcal{M}$) of the SRSPM in closed form, and discuss its salient features. For a given architecture and orientation, the singularity manifold is shown to reduce to a cubic surface $\mathcal{S}_{\boldsymbol{p}} \in \Re^3$. A complete geometric characterization of the surface, and its explicit parameterization are obtained in the following discussion. Further, using the Rodrigue's parameters (c_1, c_2, c_3) to represent orientation, we show that for a given architecture and position, $\mathcal{M}$ reduces to a 6th degree surface $\mathcal{S}_{\mathcal{O}}$ in the local coordinates c_i. Finally, using the *ball parameters* (see Appendix A for details), we derive the set of rotation angles that lead to a singularity for a given axis of rotation.

4.1 Derivation of the singularity manifold

The singularity manifold $\mathcal{M}$ is defined by the equation (9) in section 2 and is given as $D_{\boldsymbol{H}1} = \det(\boldsymbol{H}_1) = 0$. The computation of the determinant of the 6×6 matrix $\boldsymbol{H}_1$ presents great difficulties. In reference [22], the authors point out the problems of relying on the default determinant computation routines of a CAS, and come up with a *customized* procedure based on recursive cofactor expansions. In reference [23], the authors use a similar algorithm and report that the singularity manifold can be obtained via a cascade of 590 coefficients for a general SPM, and in [13], the authors report obtaining the singularity condition via a computation of 3981 symbolic determinants. In this paper, we have done all the symbolic computations in the CAS `Mathematica` [24][5], and we obtain $\det(\boldsymbol{H}_1)$ in a non-simplified form using the default routine `Det`. The size of the `Mathematica` expression of the determinant is quite large, of the order 2.7 MB. However, we are able to simplify the same using the procedures described in section 3.

The algebraic variables appearing in $\det(\boldsymbol{H}_1)$ are $\boldsymbol{x} = (r_t, c_1, c_2, c_3, x, y, z)$ and the trigonometric variables are $\boldsymbol{\gamma} = (\gamma_b, \gamma_t)$. However, $\det(\boldsymbol{H}_1)$ is a rational function in c_i due to the parameterization of $\boldsymbol{R}$ used (see equation (40) in Appendix A), and we need to rationalize it first in order to use our simplification schemes. Noting that the only denominator in $\boldsymbol{R}$ (and in $\det(\boldsymbol{H}_1)$) is $(1+c_1^2+c_2^2+c_3^2)$, we replace it by a dummy variable c_0, and multiply $\boldsymbol{H}_1$ by c_0 to get rid of all denominators. We now study the algebraic structure of $\det(c_0\boldsymbol{H}_1)$ using the monomial-based canonical form, and find that it is of degree 6 in c_i, and degree 3 in x, y, z, and degree 6 in r_t. To isolate the orientation parameters, we construct next the hybrid canonical form with r_t, x, y, z as primary variables, and c_1, c_2, c_3, c_0 as secondary variables. This results in a coefficient array of 71 elements, whose total size is about 324 MB in the non-simplified form. After simplification, only 24 non-zero coefficients remain, while the rest are identified as zero. Further, from the power vector, it is possible to identify the common factor r_t^3 among its elements, which is canceled off subsequently (r_t can not be zero for a top platform of non-zero dimension). Similarly, the coefficients have c_0 as their common factor, which is also canceled off, as c_0 being a sum of squares of real numbers, can never be zero. Next, we substitute the actual expression of c_0 into the coefficients, and simplify each of these to their monomial-based canonical forms with respect to the variables c_1, c_2, c_3. These steps reduce the size of the coefficient vector drastically from 324 MB to about 1MB, though no further cancellation of non-zero factors can be performed at the last stage. Since all the trigonometric simplifications are complete in a deterministic sense at this stage, we use the heuristic `Simplify` command of `Mathematica`. This results in another remarkable contraction of the coefficients, bringing them down to about 45 KB which is approximately *one page* of `Mathematica` textual output. It is also possible to recognize the common factor $\frac{27}{4}(1 + c_1^2 + c_2^2 + c_3^2)^3$ among the simplified coefficients at this stage, which we cancel off. The singularity condition, i.e., the equation for $\mathcal{M}$ is now obtained in terms all the manipulator parameters in a simplified form. The split of algebraic variables now needs to be changed for constructing the two singularity surfaces. In particular, to define $\mathcal{S}_{\boldsymbol{p}}$, the singularity condition is reconstructed in the hybrid form, with only x, y, z as the primary variables, and r_t, c_1, c_2, c_3 as the secondary variables. After simplification, this final form reduces to 16 monomials, whose coefficients take only about 43 KB in `Mathematica`. The highest degree of these monomials is found to be 3. Similarly, to construct $\mathcal{S}_{\mathcal{O}}$, we construct the hybrid canonical form with only c_1, c_2, c_3 as the primary variables, resulting in a 6th degree polynomial, with 77

[5]We have used Mathematica version 5.1 for 64 bit Linux (x86_64) on a PC with a single AMD Athlon 3200+ processor running at 2.0 GHz, and 2 GB of RAM.

monomials, having a total size of about 165 KB.

It is therefore obvious that further manipulation, and solution of equation (9) would be much easier in terms of the position variables, than in terms of c_i, i.e., the description of $\mathcal{S}_{\boldsymbol{p}}$ would be much simpler than that of $\mathcal{S}_{\mathcal{O}}$.

In the following, we explain discuss the properties of $\mathcal{S}_{\boldsymbol{p}}$ and $\mathcal{S}_{\mathcal{O}}$ respectively.

4.2 The singularity surface in the Cartesian space

As discussed above, the singularity condition in equation (9) can be reduced to the following polynomial equation for a given set of architectural parameters r_t, γ_b, γ_t and orientation parameters c_i:

$$\begin{aligned}\mathcal{S}_{\boldsymbol{p}} \triangleq & E_1x^2z + E_2x^2 + E_3xyz + E_4xy + E_5xz^2 + E_6xz + E_7x + E_8y^2z + E_9y^2 + E_{10}yz^2 + \\ & E_{11}yz + E_{12}y + E_{13}z^3 + E_{14}z^2 + E_{15}z + E_{16} = 0 \end{aligned} \tag{20}$$

The E_i's are the simplified coefficients of the nested canonical form in the algebraic variables(r_t, c_1, c_2, c_3) and in trigonometric variables γ_b, γ_t. The Stewart platform is in a singular configuration if the coordinates of the center of the top platform, (x, y, z), satisfy the above equation.

4.2.1 Comparison with existing results

Equation (20) is similar to those presented in [22, 12, 17, 23, 13], but is not exactly the same. In particular, the degree of the singularity expression in [22] is 4, with 32 monomials. In [12], the expression is much tighter, with 20 monomials, and degree 3 for the general case. In the case of the SRSPM, we show above that 4 of these monomials (in particular, x^3, x^2y, xy^2, y^3) vanish, resulting in an expression that is cubic in z alone, and quadratic in x, y. The least number of monomials is presented in [17], where the expression of the determinant of inverse Jacobian has two monomials (x^2z, y^2z) less than what we have in equation (20). The variation in the reported algebraic structure of the singularity condition can be attributed mainly to the following facts:

- Frames of reference and the structure of the SPM's considered in these works are not identical. As the authors point out in [22], some of their coefficients vanish in different frames of reference. In [23], the authors discuss the algebraic structure of the singularity equation for various SPM structures and point out which terms vanish for different architectures.

- In the above works, the final singularity expressions are obtained via a sequence of steps, and therefore it is quite possible that some actual zero coefficients are not identified as zeros due to incomplete simplification in the intermediate steps. This fact is apparent in the higher degree of the equation reported in [22] than in others.

In [23], from Table 1, the singularity manifold for an SRSPM is defined as polynomial which is cubic in z and quadratic in x and y. After removing the cubic terms x^3, x^2y, xy^2, y^3 in their general equation the number of coefficients in the polynomial matches with our result. However, the explicit coefficients are not derived (and the further simplification to the family of hyperbolas, with its degeneracy to parabola and straight lines is not carried out) in [23] (see Section 4.2.2 for details). The closest geometric result, to the best of our knowledge, is given by [21] where the

authors have shown that the singularity manifold of a *planar* three-degree-of-freedom manipulator consists of various conic sections, including ellipse, hyperbola and parabola.

In this paper, we have derived E_i 's *explicitly* in terms of the architecture, and orientation parameters, and we obtain compact closed form expressions for the coefficients. To illustrate the the compactness of the final forms of these expressions, we write below the coefficients of z^3, z^2, and z respectively:

$$\begin{aligned}
E_{13} =& 8\left({c_1}^2+{c_2}^2-{c_3}^2-1\right)\left({c_1}^2+{c_2}^2+{c_3}^2+1\right)\sin^3(\gamma)\left(\left({c_3}^2-1\right)\cos(\gamma)-2c_3\sin(\gamma)\right)\\
E_{14} =& 8({c_1}^2+{c_2}^2-{c_3}^2-1)r_t\sin(\gamma+3\gamma_t)((c_3{c_1}^3-3c_2{c_1}^2-3{c_2}^2c_3c_1+{c_2}^3)\cos(\gamma+3\gamma_t)+\\
& ({c_1}^3+3c_2c_3{c_1}^2-3{c_2}^2c_1-{c_2}^3c_3)\sin(\gamma+3\gamma_t))\sin^2(\gamma)+8({c_1}^2+{c_2}^2+{c_3}^2+1)\sin(2\gamma+3\gamma_t)\\
& ((c_3{c_1}^3+3c_2{c_1}^2-3{c_2}^2c_3c_1-{c_2}^3)\cos(2\gamma+3\gamma_t)-({c_1}^3-3c_2c_3{c_1}^2-3{c_2}^2c_1+{c_2}^3c_3)\times\\
& \sin(2\gamma+3\gamma_t))\sin^2(\gamma) \qquad (21)\\
E_{15} =& -8({c_1}^2+{c_2}^2)({c_1}^2+{c_2}^2-{c_3}^2-1){r_t}^2\sin(\gamma)((\left({c_3}^2-1\right)\cos(\gamma)-2c_3\sin(\gamma))\sin^2(\gamma+3\gamma_t)+\\
& 8({c_1}^2+{c_2}^2)({c_1}^2+{c_2}^2+{c_3}^2+1)\sin(\gamma)((\left({c_3}^2-1\right)\cos(\gamma)-2c_3\sin(\gamma))\sin^2(2\gamma+3\gamma_t)+\\
& ({c_1}^2+{c_2}^2)r_t(-4{c_3}^3+4(\left({c_3}^2-1\right)\cos(4\gamma)c_3+4c_3-2({c_3}^2+1)^2\sin(2\gamma)+\\
& 4\cos(6\gamma_t)((\left({c_3}^2-1\right)\cos(\gamma)-2c_3\sin(\gamma))^2(\sin(2\gamma)-\sin(4\gamma))+(3{c_3}^4-2{c_3}^2+3)\sin(4\gamma)+\\
& 8(2\cos(2\gamma)+1)\sin^2(\gamma)(-\cos(\gamma){c_3}^2+2\sin(\gamma)c_3+\cos(\gamma))^2\sin(6\gamma_t))
\end{aligned}$$

where $\gamma = \gamma_b - \gamma_t$. It can be noted that the explicit functional dependence of the coefficients is easily seen in the above expressions.

Some existing results in singularity of the SRSPM can be readily obtained from these expressions:

- Architecture singularity [14]: It can be seen that E_{13}, E_{14} and E_{15} vanish when $\sin\gamma = 0$, i.e., $\gamma_b = \gamma_t$, and the two platforms are *similar*. Indeed, all E_i 's vanish under this condition. Therefore the manipulator is singular at *all possible configurations*, i.e., it is architecturally singular.

- Fichter's singularity [4]: When the top platform is horizontal, we have $c_1 = c_2 = 0$, $c_3 = \tan(\theta_z/2)$, $\theta_z \in [0, 2\pi]$ being the rotation about the vertical axis. Upon substituting these conditions, all E_i 's vanish except E_{13}, and from equations (20,21), we have

$$8(c_3^2+1)^2\sin^3(\gamma)((1-c_3^2)\cos(\gamma)+2c_3\sin(\gamma))z^3 = 0 \qquad (22)$$

  Ignoring the possibilities of architectural singularity($\gamma = 0$) and the coplanarity of the two platforms ($z = 0$), the only real solution of equation (22) is $\theta_z = \gamma \pm \pi/2$. The top platform is aligned with the bottom when $\theta_z = \gamma$, therefore $\theta_z = \gamma \pm \pi/2$ implies that the top platform is rotated by $\pm\pi/2$ with respect to the bottom about the vertical axis, which is the singular configuration reported by Fichter.

4.2.2 Geometric characterization of the singularity surface $\mathcal{S}_p$

Equation (20) describes the singularity surface $\mathcal{S}_p$ for a given set of architectural parameters r_t, γ_b, γ_t, and a given orientation c_1, c_2, c_3. We observe that $\mathcal{S}_p$ is cubic in z and quadratic in x, y. Therefore, absorbing the z-terms into the coefficients of power-products of x, y, we can re-write equation (20) as

$$\mathcal{C} \triangleq ax^2 + 2hxy + by^2 + 2gx + 2fy + c = 0 \qquad (23)$$

Equation (23) implies that each z-section of $\mathcal{S}_{\boldsymbol{p}}$ is a *conic section*. The coefficients of the standard form of the conic section, namely a, b, h, g, f, and c, were expressed in terms of E_i, z. It is well known that all the properties of a conic section can be derived in terms of the coefficients a, b, h, g, f, and c. Most importantly, we can associate a function $\delta = h^2 - ab$ with the conic section $\mathcal{C}$, and note that $\mathcal{C}$ defines an ellipse if $\delta < 0$, a parabola if $\delta = 0$, and a hyperbola if $\delta > 0$ respectively. Casting δ as a polynomial in z, we find that δ is a quadratic of the form:

$$\delta = e_0 z^2 + e_1 z + e_2 \tag{24}$$

The sign of δ depends on the value of the discriminant $\Delta = e_1^2 - 4e_0e_2$. Simplifying to the nested canonical form with respect to r_t, x, y, it is observed that Δ is *zero identically*. Therefore, δ is a perfect square of the form

$$\delta = (z - z_{\mathrm{p}})^2,\ z_{\mathrm{p}} = -\frac{e_1}{2e_0} \tag{25}$$

The above equation implies that $\delta \geq 0$, and hence $\mathcal{C}$ *can not be an ellipse at any section*. In particular, it is a hyperbola in each horizontal section, apart from a unique section at $z = z_{\mathrm{p}}$ where it is a parabola. Expression of z_{p} is given in terms of the manipulator parameters as:

$$\begin{aligned} z_{\mathrm{p}} =& ((1 + c_3^2) r_t \sin(\gamma + 3\gamma_t)(-c_1^3 + 3c_1c_2^2 - 3c_1^2c_2c_3 + c_2^3c_3)\cos(\gamma + 3\gamma_t) + \\ & (-3c_1^2c_2 + c_2^3 + c_1^3c_3 - 3c_1c_2^2c_3)\sin(\gamma + 3\gamma_t))/ \\ & \big(\sin(\gamma)(c_1^2 + c_2^2)(1 + c_1^2 + c_2^2 + c_3^2)(2c_3\cos(\gamma) + (c_3^2 - 1)\sin(\gamma))\big) \end{aligned} \tag{26}$$

We can also conclude that the curve $\mathcal{C}$, and hence the surface $\mathcal{S}_{\boldsymbol{p}}$ is *unbounded*.

It is also possible for the hyperbolas to *degenerate* to a pair of straight lines. Since all the E_i's are differentiable functions, the surface $\mathcal{S}_{\boldsymbol{p}}$ is smooth and extends infinitely in the Z direction, the only possibility of such degeneracy is when the hyperbola gradually deforms into its asymptotes, and continue to deform to reappear as a hyperbola that is *conjugate* to the one prior to the degeneracy. The condition for this is given by:

$$\det \begin{pmatrix} a & h & g \\ h & b & f \\ g & f & c \end{pmatrix} = 0 \tag{27}$$

Expanding the determinant, we cast it as polynomial in z, and it turns out to be a quintic:

$$f_0 z_1^5 + f_1 z_1^4 + f_2 z_1^3 + f_3 z_1^2 + f_4 z_1 + f_5 = 0 \tag{28}$$

Simplifying f_i to the nested polynomial form in r_t, and c_i, we find that $f_0 = 0$, i.e., equation (28) is a quartic in reality. It is still difficult to obtain the number of real solutions for z_1 due to the complexity of f_i. However, we conclude the following: $\mathcal{S}_{\boldsymbol{p}}$ *can degenerate into a pair of straight in* 0, 2 *or* 4 *planes defined by* $z = z_1$. *In these sections alone the two sheets of* $\mathcal{S}_{\boldsymbol{p}}$ *meet at a point, as major axis of the hyperbolas change from* X *to* Y *or vice-versa.*

It may be noted that this geometric characterization is possible due to the compact nature of the coefficients, E_i's and use of the simplification algorithms described in section 3. In particular, the simplification of Δ, f_0 to zero demonstrates a situation where such computations help reveal the true algebraic structure of a problem, and substantiates the claims made in section 3 about the utility of our simplification algorithms.

Consequences of this geometric characterization are as follows:

- It is possible to obtain an algebraic parameterization of $\mathcal{S}_{\boldsymbol{p}}$. Apart from the sections $z = z_{\rm p}$ or $z = z_{\rm l}$, the surface cuts each z-plane in a hyperbola. Choosing one parameter as z, it remains to parameterize the hyperbolas in each z plane. The hyperbolas can first be transformed into their canonical forms via a rotation and translation of their individual planes. The *center* of $\mathcal{C}$ is given by

$$\begin{aligned} x_0 &= \frac{bg - fh}{h^2 - ab} \\ y_0 &= \frac{gh - af}{h^2 - ab} \end{aligned} \tag{29}$$

  and the orientation of the axes of the hyperbolas in the global frame can be given by

$$\theta_c = \text{atan2}(a - b, 2h) \tag{30}$$

  where $atan2(x, y)$ is the two-argument inverse tangent function. In the canonical form, assuming X as the major axis, hyperbolas admit the parameterization $x = \frac{a'}{2}(t + \frac{1}{t}), y = \frac{b'}{2}(t - \frac{1}{t})$ for the part on the right of the origin, and $x = -\frac{a'}{2}(t + \frac{1}{t}), y = -\frac{b'}{2}(t - \frac{1}{t})$ for the other. The constants a', b' can be obtained from the coefficients in equation (23). The curves approach their asymptotes as $t \to 0$, and cut the major axis when $t = 1$. We define a *bounding box* in each plane, whose length is given by sa' along the major axis, where $s > 1$ can be chosen as per convenience of visualization. Accordingly, the parameter t varies from $s - \sqrt{s^2 - 1}$ to $s + \sqrt{s^2 - 1}$. A similar parameterization can be obtained when Y is the major axis. Therefore the pair (z, t) forms an explicit 2-parameter description of $\mathcal{S}_{\boldsymbol{p}}$.

- Topology of the nonsingular subspace of $\Re^3$ at a given architecture and orientation can be complicated, and possibly vary from case to case. For example, the *central portion* of the hyperbolas, containing (x_0, y_0) in each plane, collapses to a point at each section the hyperbolas degenerate to a pair of intersecting straight lines. As the hyperbolas extend to infinity, each of these portions are *separated* from the rest of $\Re^3$ by the singularity manifold. However, as explained above, the number of such sections can be 0, 2 or 4, and further, some of these sections may not be realizable in a physical sense (e.g., if the section is *not* between the two platforms, such that $z_{\rm l} < 0$ in our case). Moreover, there is a single plane $z = z_{\rm p}$, in which one of the parts of the hyperbola transforms into a parabola, while the other vanishes, thereby providing a *corridor* connecting the two subspaces of $\Re^3$ otherwise separated by it. Various combinations of the feasible (i.e., positive) values of $z_{\rm p}$ and $z_{\rm l}$ lead to different topologies of the non-singular subspaces.

It is also possible to identify certain horizontal planes where the coefficients of $\mathcal{C}$ show some more special properties. We list some of them below:

- $a + b = 0$ (Rectangular hyperbola):

$$\begin{aligned} z =& r_t(1 + c_3^2)\sin(\gamma + 3\gamma_t)((-3c_1^2c_2 + c_2^3 + c_1^3c_3 - 3c_1c_2^2c_3)\cos(\gamma + 3\gamma_t) + \\ & (c_1^3 + (-3c_1c_2^2 + 3c_1^2c_2c_3 - c_2^3c_3)\sin(\gamma + 3\gamma_t))/ \\ & (\sin(\gamma)(c_1^2 + c_2^2)(1 + c_1^2 + c_2^2 + c_3^2)((c_3^2 - 1)\cos(\gamma) - 2c_3\sin(\gamma))) \end{aligned} \tag{31}$$

- $a = b$ ($\theta_c = \frac{\pi}{2}$, the global Y axis is the major axis of the hyperbola):

$$\begin{aligned} z =&(c_1^2 + c_2^2) r_t \sin(\gamma + 3\gamma_t)((c_2 - 3c_2c_3^2 + c_1c_3(-3 + c_3^2)) \cos(\gamma + 3\gamma_t) + \\ &(c_2c_3(-3 + c_3^2) + c_1(-1 + 3c_3^2)) \sin(\gamma + 3\gamma_t))/ \\ &(\sin(\gamma)(1 + c_3^2)(1 + c_1^2 + c_2^2 + c_3^2)((c_1^2 - c_2^2) \cos(\gamma) - 2c_1c_2 \sin(\gamma))) \end{aligned} \tag{32}$$

- $h = 0$ ($\theta_c = 0$, the global X axis is the major axis of the hyperbola):

$$\begin{aligned} z =&r_t(c_1^2 + c_2^2) \sin(\gamma + 3\gamma_t)((c_1 - 3c_1c_3^2 - c_2c_3(c_3^2 - 3)) \cos(\gamma + 3\gamma_t) + \\ &(c_2 - 3c_2c_3^2 + c_1c_3(c_3^2 - 3)) \sin(\gamma + 3\gamma_t))/ \\ &(\sin(\gamma)(1 + c_3^2)(1 + c_1^2 + c_2^2 + c_3^2)(2c_1c_2 \cos(\gamma) + (c_1^2 - c_2^2) \sin(\gamma))) \end{aligned} \tag{33}$$

4.3 Singularity surface in the orientation parameters

We now describe a complimentary representation of $\mathcal{M}$, which is a surface in the local coordinates of $SO(3)$ for a given architecture and position. The surface, denoted by $\mathcal{S}_{\mathcal{O}}$, is such that every point on it corresponds to an orientation which is singular, and for a given architecture and position, *all* such orientations lie on this surface. We note that this representation of $\mathcal{M}$ is not studied very well and the closest work is by Li et al. [13] where a numerical example is presented.

We start by recollecting the equation defining $\mathcal{S}_{\mathcal{O}}$ which was obtained as a polynomial consisting of 77 monomials in c_i, including the constant term. The corresponding coefficients are functions of the architecture and position parameters of the manipulator. The highest exponents in terms of c_i are $5, 5$, and 6 respectively, and the total degree of the corresponding equation in c_i is 6. Moreover, although c_i provides a very effective means to derive $\mathcal{S}_{\mathcal{O}}$ in closed form, it is difficult to visualize the singularities in terms of these parameters due to the following reasons:

- For a given axis of rotation (with the sense associated), the rotation can vary from 0 to π, and therefore c_i can vary from $-\infty$ to ∞. Such infinite range of values make it inappropriate for visualization purposes.

- From a given set of c_i, it is difficult to obtain an intuitive idea of the orientation, unless it is converted to some parameter set with more apparent geometric significance.

To overcome these short-comings simultaneously, we convert the polynomial in c_i to an equivalent expression in the ball parameters via equation (43) (see Appendix A.2). Writing t_θ for $\tan(\theta/2)$, we obtain a 6-degree polynomial in t_θ as follows:

$$g_0 t_\theta^6 + g_1 t_\theta^5 + g_2 t_\theta^4 + g_3 t_\theta^3 + g_4 t_\theta^2 + g_5 t_\theta + g_6 = 0 \tag{34}$$

where θ is the rotation about the axis of the finite rotation.

The set of coefficients g_i have an one-to-one correspondence with the unit vectors emanating from the origin of $\Re^3$. Therefore each such set represents a *unique* direction and the sense of rotation, and each solution of equation (34) such that $t_\theta \in [0, \infty]$, gives the corresponding angle of CCW rotation via the transformation

$$\theta = 2 \text{ atan2}(1 + t_\theta^2, 2t_\theta) \tag{35}$$

The expressions of g_i's are complicated, hence the number of *feasible* roots of equation (34) can not be ascertained *a priori*. We can only conclude that *for a given architecture and position, there are* $0, 2, 4$ *or* 6 *CCW rotations in* $[0, \pi]$ *about any given axis such that the resulting orientation of the top platform leads to a singular configuration.* However, these rotation angles can be computed relatively easily using the analytical expressions of g_i. Moreover, as the rotation axis is made to sweep through the entire sphere $\mathbb{S}^2$ (i.e., $\alpha \in [-\pi/2, \pi/2]$, $\beta \in [0, 2\pi]$), and corresponding feasible values of θ are obtained, *all* the singular orientations can be enlisted.

It may be mentioned that the computation of orientation singularity manifold in [13] is in terms of tangent half-angles of the Euler angles. The general expressions are in terms of 3981 determinants which lead to 2173 coefficients, whereas our g_i's are in a much more simpler, explicit functional form. We present the expressions for g_4, g_5 and g_6 to illustrate this.

$$
\begin{aligned}
g_4 &= z(4z^2\cos(\gamma)\sin^2(\alpha)\sin^3(\gamma) + 4z\cos(\alpha)\sin(\alpha)(\sin(\beta)(y\cos(\gamma) + 5x\sin(\gamma)) \\
&\quad + \cos(\beta)(x\cos(\gamma) - 5y\sin(\gamma)))\sin^3(\gamma) + \cos^2(\alpha)(-4\cos(3(\gamma + 2\gamma_t)) \\
&\quad \times \cos^2(\gamma) + \cos(\gamma) + 3\cos(3\gamma) + 4\sin(\gamma)(y\sin(2\beta - \gamma - 3\gamma_t) - x\cos(2\beta - \gamma - 3\gamma_t))\sin(\gamma + 3\gamma_t)) \\
&\quad \times r_t\sin(\gamma) - 2\cos^2(\alpha)\sin(2\gamma)\sin^2(\gamma + 3\gamma_t)r_t^2 + \cos^2(\alpha)(8y^2\cos(\beta)\cos(\beta + \gamma)\sin^3(\gamma) \\
&\quad + 8x^2\sin(\beta)\sin(\beta + \gamma)\sin^3(\gamma) - 8xy\sin(2\beta + \gamma)\sin^3(\gamma) \\
&\quad - 4x\cos(2\beta - 2\gamma - 3\gamma_t)\sin(2\gamma + 3\gamma_t)\sin^2(\gamma) + 4y\sin(2\beta - 2\gamma - 3\gamma_t)\sin(2\gamma + 3\gamma_t)\sin^2(\gamma) \\
&\quad - 2\sin(2\gamma)\sin^2(2\gamma + 3\gamma_t))) \\
g_5 &= 4z^2\sin^3(\gamma)(2z\sin(\alpha)\sin(\gamma) + \cos(\alpha)(\cos(\beta)(x\sin(\gamma) - 3y\cos(\gamma)) \\
&\quad + \sin(\beta)(3x\cos(\gamma) + y\sin(\gamma)))) \\
g_6 &= 4z^3\cos(\gamma)\sin^3(\gamma)
\end{aligned}
\tag{36}
$$

As in the case of $\mathcal{S}_{\boldsymbol{p}}$, we observe that for two similar platforms with $\gamma = 0$ ($\gamma_b = \gamma_t$), g_4, g_5 and g_6 are zero. Indeed, all g_i 's vanish under this condition, and the manipulator is singular at *all possible configurations*, i.e., it is architecturally singular.

4.4 Illustrative examples

In this section, we plot the surfaces $\mathcal{S}_{\boldsymbol{p}}$ and $\mathcal{S}_{\mathcal{O}}$ for a SRSPM to illustrate the results described above. The geometry of the top and bottom platforms are taken to be the same as the INRIA prototype [22, 23, 13]. However, the top platform is mobile in our case, and all the lengths are scaled such that the radius of the bottom platform is unity. The resulting architectural parameters of this manipulator are as follows:

$$r_t = 0.5803, \quad \gamma_b = 0.2985\text{rad}, \quad \gamma_t = 0.6573\text{rad}$$

and therefore $\gamma = -0.3588$rad. The manipulator is shown in figure 2 below in a reference configuration, where $x = y = 0$, $z = 1$, and $\boldsymbol{R} = \boldsymbol{R}_z(\gamma)$, such that the axes of symmetry in the two platforms are vertically aligned. In the following, we present the surfaces $\mathcal{S}_{\boldsymbol{p}}$ and $\mathcal{S}_{\mathcal{O}}$ respectively for this manipulator.

4.4.1 Examples of $\mathcal{S}_{\boldsymbol{p}}$

We choose two different orientations to illustrate $\mathcal{S}_{\boldsymbol{p}}$. First we take $c_1 = 0.4, c_2 = 0.2, c_3 = 0.6$. A part of the corresponding surface is shown in figure 3. For this case, $z_{\text{p}} = 0.4026$,

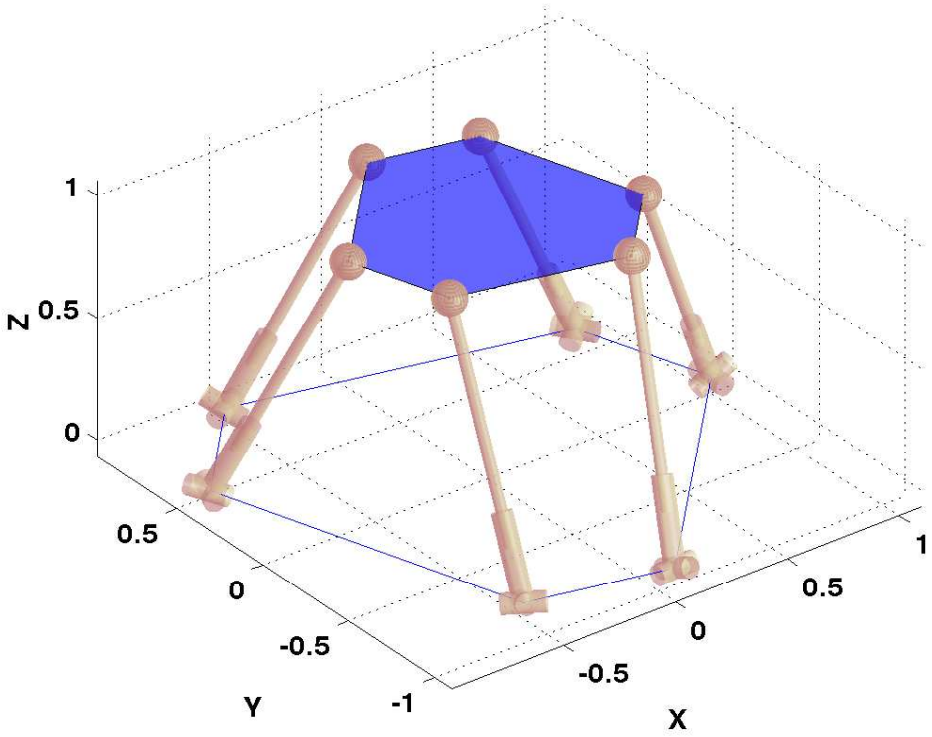

Figure 2: The SRSPM in a reference configuration

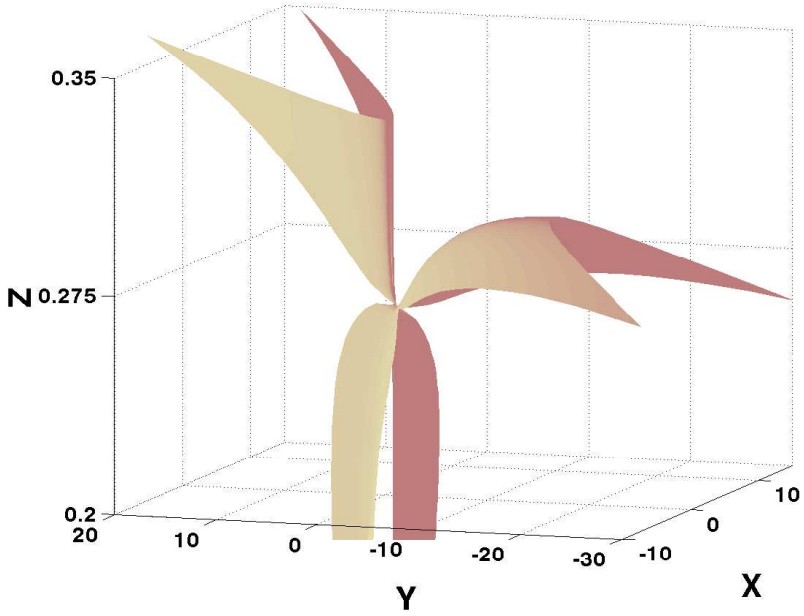

Figure 3: $\mathcal{S}_{\boldsymbol{p}}$ for $c_1 = 0.4, c_2 = 0.2, c_3 = 0.6$

and the heights at which the hyperbolas degenerate to pairs of straight lines are given by $z_{\mathrm{l}} = (-0.2390, 0.2692, 0.7675, 0.9413)$. We can see that the two sheets of $\mathcal{S}_{\boldsymbol{p}}$ meet at $z = 0.2692$, and then start moving away from each other rapidly as the height approaches $z_{\mathrm{p}} = 0.4026$. The variation of the major and minor axis lengths shown in figure 4(a) represent these trends quantitatively. The dotted horizontal line indicates the direction of the major axis, with 0 implying the X-axis, and 1 implying Y. It can be seen clearly that the major and minor axes of the hyperbola interchange at $z = 0.2692$, and as it approaches the parabolic section, the major axis of the hyperbola starts increasing rapidly. The center also moves rapidly away from its initial position, such that its locus becomes nearly horizontal.

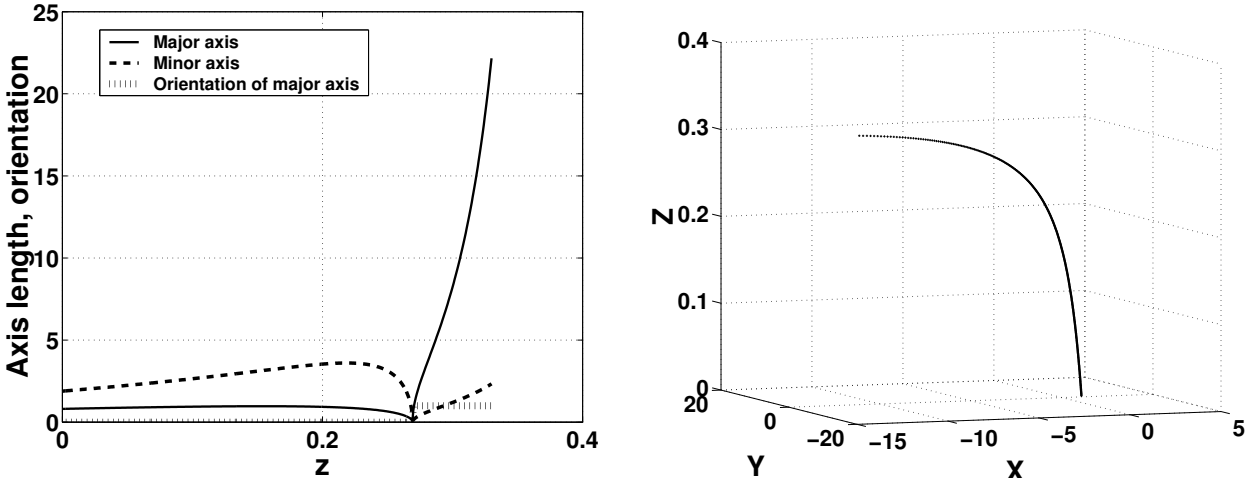

(a) Variation of the major and minor axis

(b) Locus of the center of the conic section $\mathcal{C}$

Figure 4: Properties of the conic section $\mathcal{C}$ at various z-sections ($c_1 = 0.4, c_2 = 0.2, c_3 = 0.6$)

The second example is chosen such that $c_1 = 0, c_2 = 0.1, c_3 = 0.1$. This combination illustrates the multiple cross-overs of the two sheets of $\mathcal{S}_{\boldsymbol{p}}$ clearly. Two views of the surface are shown in figure 5(a) and figure 5(b) respectively.

The parabolic section in this case is located at $z = -0.3041$, and the interchange of axes takes place at $z = (-0.2448, -0.0919, 0.0810, 0.4528)$. In figures 6(a) and 6(b), we see the variation of the axis lengths, and the locus of the center of $\mathcal{C}$.

4.4.2 Example of $\mathcal{S}_{\mathcal{O}}$

To illustrate the surface $\mathcal{S}_{\mathcal{O}}$, we use the position $x = y = 0$, and $z = 1$. It is difficult to plot the surface, as no explicit parameterization has been obtained in this case. However, we evaluate the points on $\mathcal{S}_{\mathcal{O}}$ numerically, and plot them together. Figure 7 shows such a plot of $\mathcal{S}_{\mathcal{O}}$. It can be seen that the surface seems repeated thrice along the β axis. To get a better view of the surface, we look into one-third of it in greater detail in figure 8. Figure 9 presents another view of the same part of $\mathcal{S}_{\mathcal{O}}$.

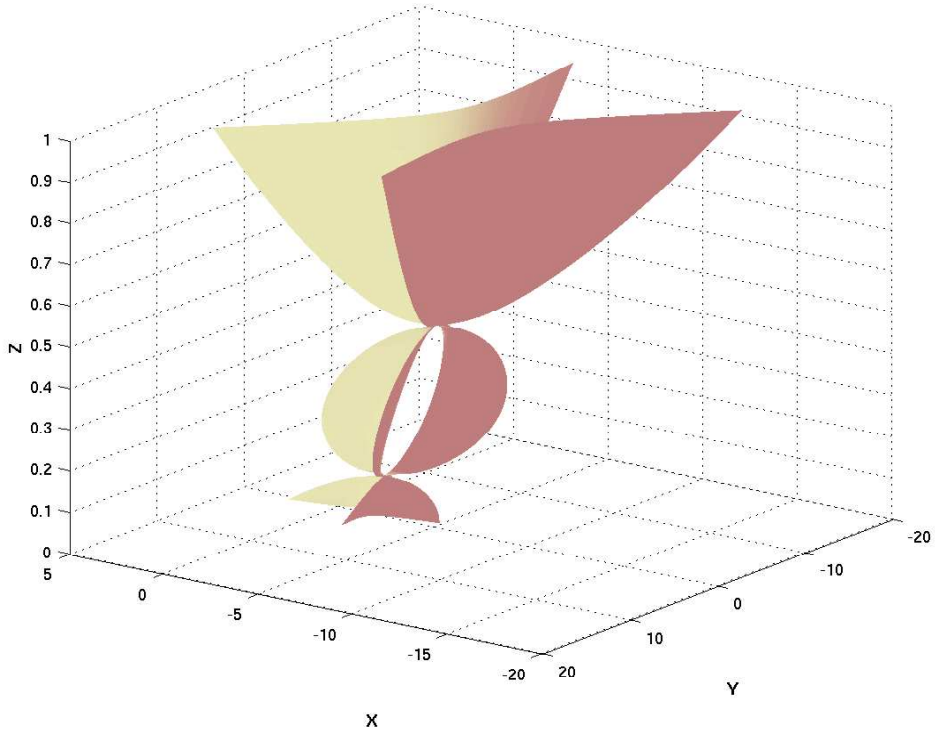

(a) View 1

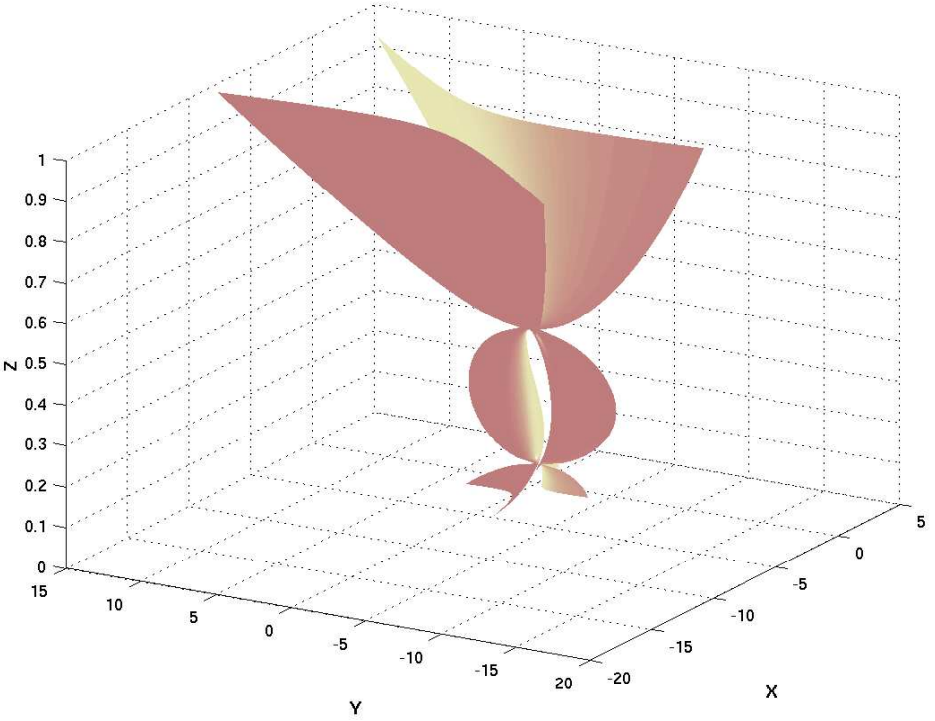

(b) View 2

Figure 5: Two views of $\mathcal{S}_{\boldsymbol{p}}$ for $c_1 = 0, c_2 = 0.1, c_3 = 0.1$

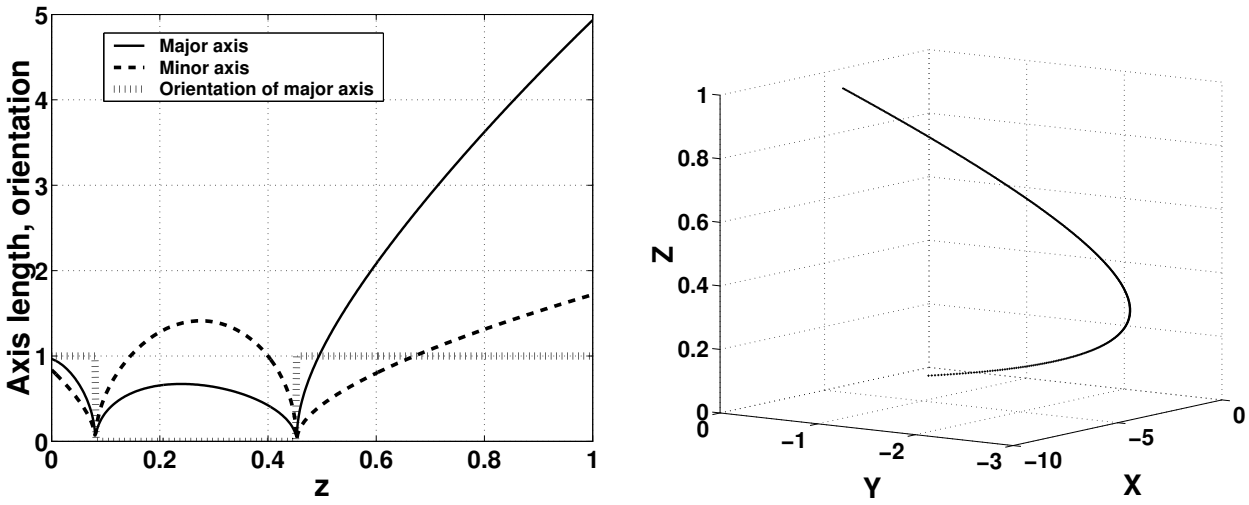

(a) Variation of the major and minor axis

(b) Locus of the center of the conic section $\mathcal{C}$

Figure 6: Properties of the conic section $\mathcal{C}$ at various z-sections ($c_1 = 0, c_2 = 0.1, c_3 = 0.1$)

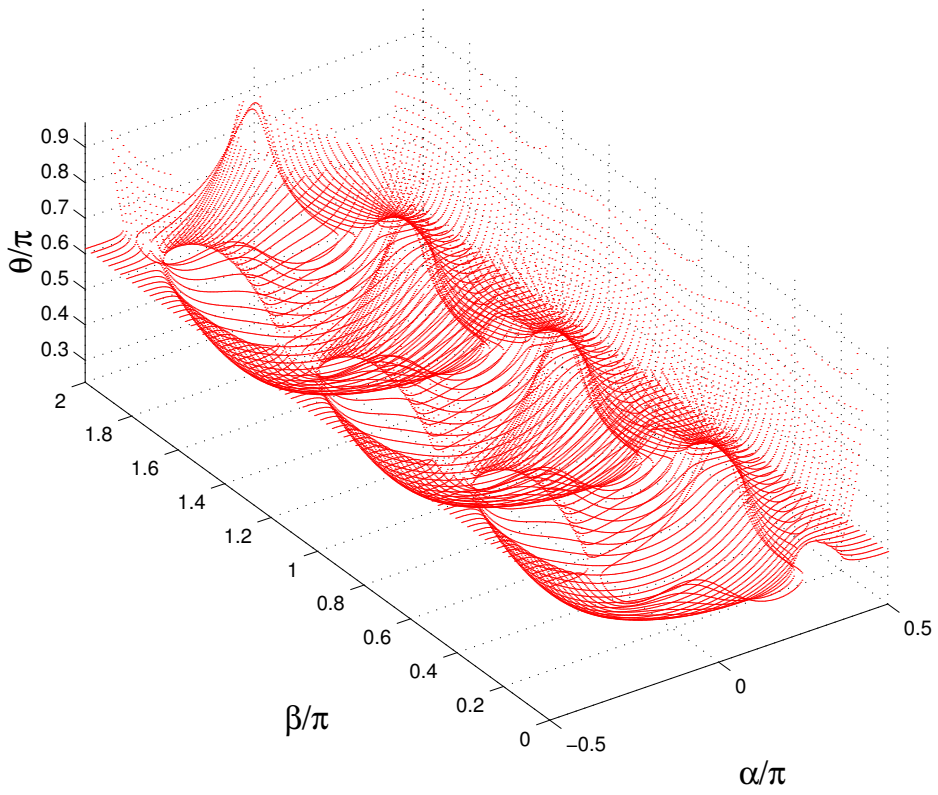

Figure 7: A view of $\mathcal{S}_{\mathcal{O}}$ at $x = y = 0, z = 1$

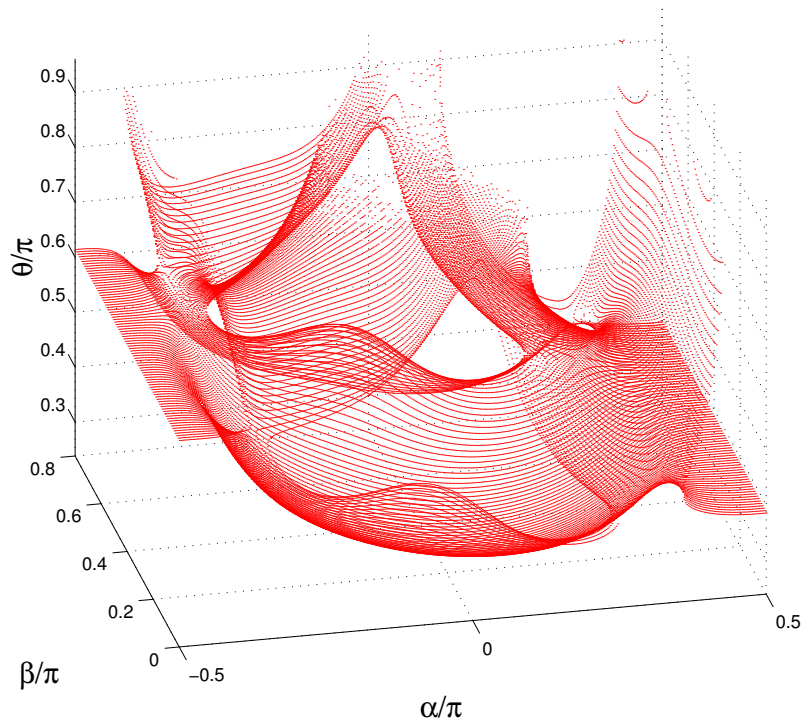

Figure 8: View of a part of $\mathcal{S}_{\mathcal{O}}$ at $x = y = 0, z = 1$

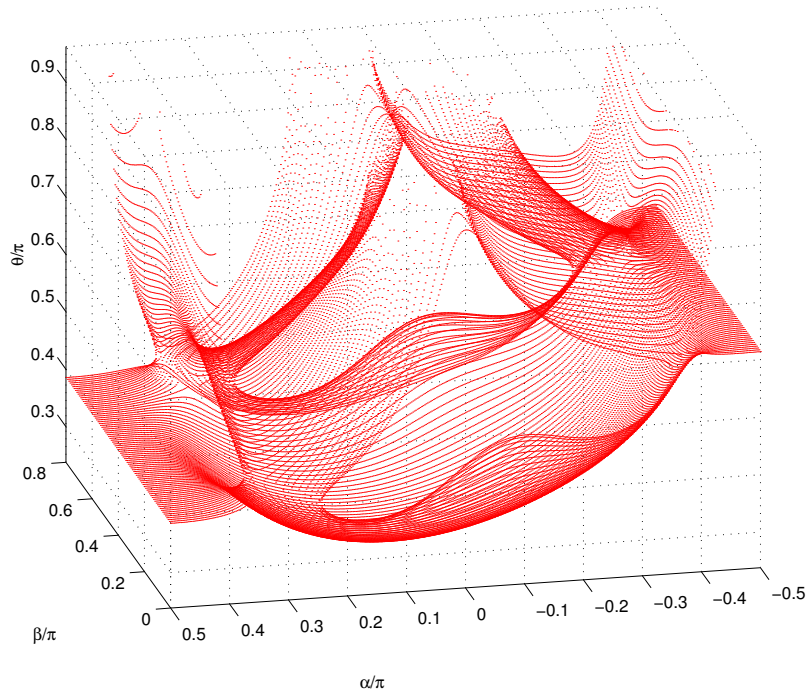

Figure 9: Another view of a part of $\mathcal{S}_{\mathcal{O}}$ at $x = y = 0, z = 1$

5 Examples of singular configuration

We present a few examples of a singular configuration of the SRSPM. We use the same architecture as in section 4.4. The orientation of the top platform is also chosen as in the examples of $\mathcal{S}_{\boldsymbol{p}}$, and the position is set to $x = y = 0$. The z component of position is obtained from equation (20), which yields 3 solutions for each set of x, y and other parameters. We use only the positive values of z in the following.

Example 1: We choose $x = y = 0, c_1 = 0.4, c_2 = 0.2, c_3 = 0.6$ and evaluate a singularity corresponding to $\mathcal{S}_{\boldsymbol{p}}$. For these numerical values, equation (20) reduces to

$$\begin{aligned}&-0.1115z^3 + 0.0533xz^2 + 0.3502yz^2 + 0.0478z^2 + 0.1046x^2z - 0.1431y^2z\\&-0.3778xz + 0.1582xyz - 0.2817yz + 0.2994z + 0.0266x^2 + 0.0854y^2 + 0.0988x\\&-0.1512xy + 0.0046y - 0.1550 = 0\end{aligned}$$

Substituting $x = y = 0$ in the above polynomial, we get

$$-0.1115z^3 + 0.0478z^2 + 0.2994z - 0.1550 = 0$$

and the solution of the above cubic gives $z = 0.5282, 1.5735, -1.6732$. For the two positive z values the manipulator configurations are shown in figures 10(a) and 10(b) respectively.

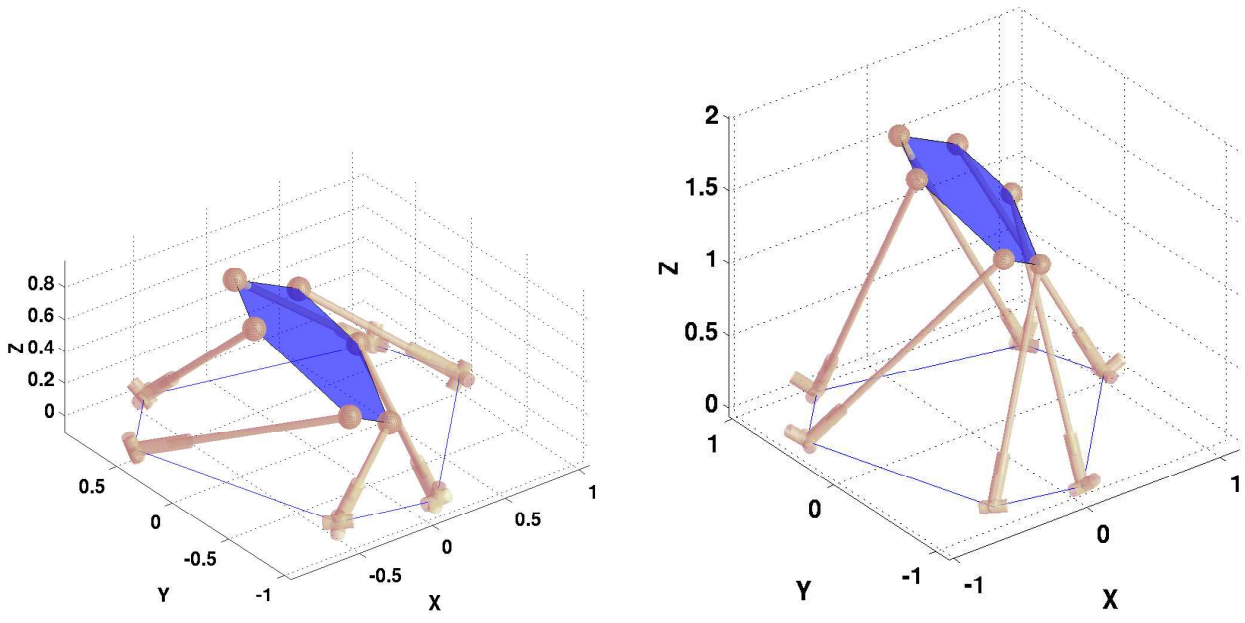

(a) $z = 0.5282$ (b) $z = 1.5735$

Figure 10: Singular configurations of the SRSPM at $x = y = 0, c_1 = 0.4, c_2 = 0.2, c_3 = 0.6$

Example 2: For the values chosen as $x = y = 0, c_1 = 0, c_2 = 0.1, c_3 = 0.1$, there is only one positive solution for z given by $z = 0.2091$. The corresponding singular configuration is shown in figure 11.

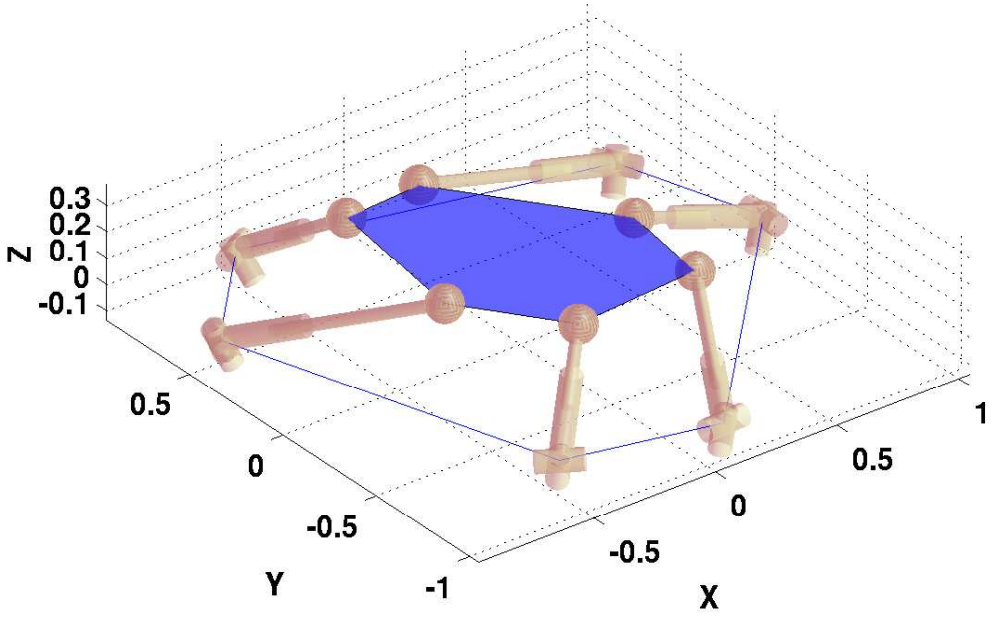

Figure 11: Singular configurations of the SRSPSM at $x = y = 0, c_1 = 0, c_2 = 0.1, c_3 = 0.1$

Example 3: We choose $x = y = 0$, $z = 0.2091$, $c_2 = 0.1, c_3 = 0.1$ and evaluate a singularity configuration corresponding to $\mathcal{S}_{\mathcal{O}}$. In this case, the position is fully prescribed, and the orientation is partially specified. The parameter c_1 is computed from the singularity condition. The values of c_1 are real and are given by $(-0.08889, 0.0000, 0.4139, 1.5384, 21.1170)$. The roots are distinct which numerically justifies our claim of deriving the minimal form of $\mathcal{S}_{\mathcal{O}}$. Further, the second configuration with $c_1 = 0.0000$ is theoretically the same as in the second example above, where c_1 was set to 0. The match of the computed solution with the exact result verifies our computations numerically. We show the set of singular configurations in figures 12(a)-12(e).

6 Conclusion

In this paper, we have presented a detailed analytical description of the singularities of a class of 6-6 Stewart platform manipulators. We have derived the analytical equations of the singularity manifold $\mathcal{M} \in SE(3)$. For a given architecture, we have decomposed $\mathcal{M}$ as surfaces $\mathcal{S}_{\boldsymbol{p}} \in \Re^3$ and $\mathcal{S}_{\mathcal{O}} \in SO(3)$, consisting of the singular configurations at a given orientation, and rotation respectively. We have also presented detailed geometric characterization of $\mathcal{S}_{\boldsymbol{p}}$, and its explicit parameterization. Such results are novel for any SPM as far as we know, and the methods used here can be applied to analysis of any SPM or similar mechanisms.

Extensive symbolic manipulations and simplifications have been used throughout the paper, and for carrying out such tasks efficiently, we have developed simplification algorithms based on three different canonical forms of algebraic-trigonometric expressions. These algorithms can simplify large expressions involving algebraic and trigonometric terms, and their applications are not limited to singularity analysis of SPMs or rigid-body kinematics.

The results presented in this paper should facilitate important functional aspects of parallel

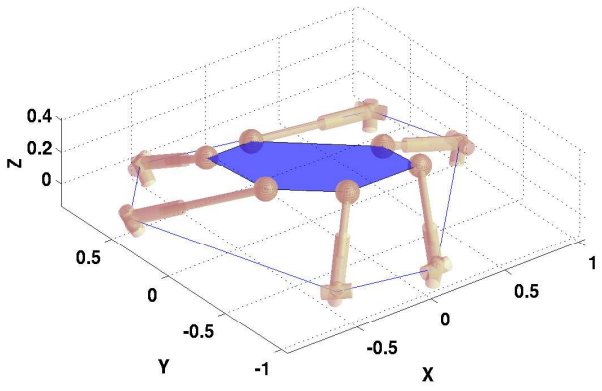

(a) $c_1 = -0.0889$

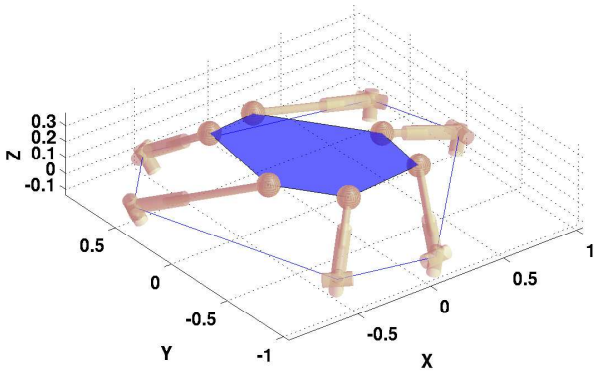

(b) $c_1 = 0.0000$

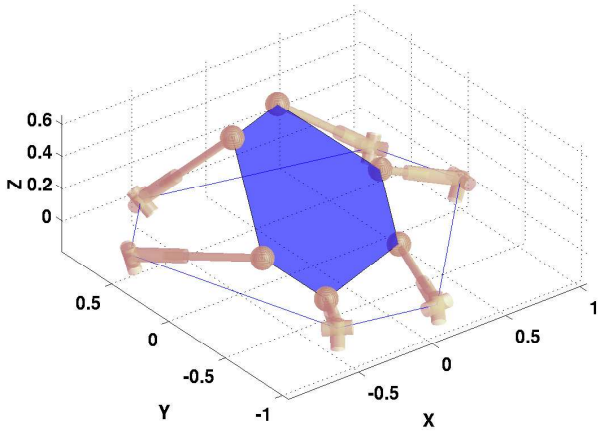

(c) $c_1 = 0.4139$

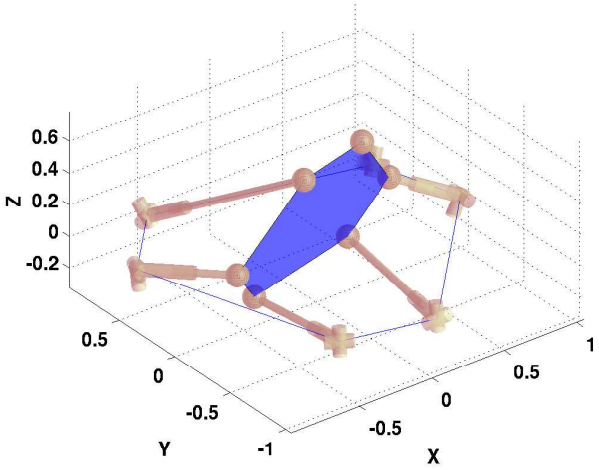

(d) $c_1 = 1.5384$

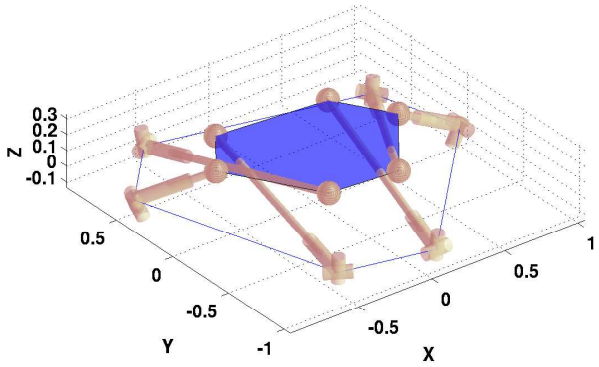

(e) $c_1 = 21.1170$

Figure 12: Singular configurations of the SRSPM at $x = y = 0, z = 0.2091, c_2 = 0.1, c_3 = 0.1$

robots, such as detection of singularities, and formal verification of trajectories. With the compact analytical conditions for singularity allowing parametric study of designs with very less computations, the task of designing singularity-free workspaces should be greatly facilitated. The methods described here can also be used without modification to study the singularities of more general forms of the SPM.

Acknowledgement

The authors wish to thank the anonymous reviewers for their valuable comments.

References

[1] Basu, D. and Ghosal, A. (1997), 'Singularity analysis of platform-type multi-loop spatial mechanisms', *Mechanism and Machine Theory*, **32**, pp. 375–389.

[2] Cohen, J. S. (2002), *Computer Algebra and Symbolic Computation: Mathematical Methods*, A K Peters, Natick.

[3] Cox, D., Little, J. and O'Shea, D. (1991), *Ideals, Varieties, and Algorithms: An Introduction to Computational Algebraic Geometry and Commutative Algebra*, Springer-Verlag, New York.

[4] Fichter, E. F. (1986), 'A Stewart platform-based manipulator: general theory and practical construction', *International Journal of Robotics Research*, **5**(2), pp. 157–182.

[5] Geddes, K. O., Czapor, S. R. and Labahn, G. (1992), *Algorithms for Computer Algebra*, Kluwer Academic Publishers, Boston.

[6] Gosselin, C. and Angeles, J. (1990), 'Singularity analysis of closed loop kinematic chains', *IEEE Transactions on Robotics and Automation*, **6**(3), pp. 281–290.

[7] Gregorio, R. D. (2001*a*), 'Analytic formulation of the 6-3 fully-parallel manipulators singularity determination', *Robotica*, **19**, pp. 663–667.

[8] Gregorio, R. D. (2001*b*), 'Statics and singularity loci of the 3-UPU wrist', *2001 IEEE/ASME International Conference on Advanced Intelligent Mechatronics Proceedings*, Italy, pp. 470–475.

[9] Gregorio, R. D. (2002), 'Singularity-locus expression of a class of parallel mechanisms', *Robotica*, **20**, pp. 323–328.

[10] Herstein, I. N. (1975), *Topics in Algebra*, John Wiley & Sons, New York.

[11] Hunt, K. H. (1978), *Kinematic Geometry of Mechanism*, Clarendon Press, Oxford.

[12] Kim, D. and Chung, W. (1999), 'Analytic singularity equation and analysis of six-dof parallel manipulators using local structurization method', *IEEE Transactions on Robotics and Automation*, **15**(4), pp. 612–622.

[13] Li, H., Gosselin, C., Richard, M. J. and St-Onge, B. M. (2004), 'Analytic form of the six-dimensional singularity locus of the general Gough-Stewart platform', *Proceedings of ASME 28th Biennial Mechanisms and Robotics Conference*, Salt Lake City, Utah, USA'.

[14] Ma, O. and Angeles, J. (1991), 'Architectural singularities of platform manipulators', *Proceedings of International Conference on Robotics and Automation*, pp. 1542–1547.

[15] McCarthy, J. M. (2002), *Geometric Design of Linkages*, Springer, New York.

[16] Merlet, J.-P. (1989), 'Singularity configurations of parallel manipulators and Grassman geometry', *International Journal of Robotics Research*, **8**, pp. 45–56.

[17] Merlet, J.-P. (2001), *Parallel Robots*, Kluwer Academic Press, Dordrecht.

[18] Miscehnko, A. and Fomenko, A. (1988), *A Course of Differential Geometry and Topology*, Mir Publishers, Moscow.

[19] Murray, R. M., Li, Z. and Sastry, S. S. (1994), *A Mathematical Introduction to Robotic Manipulation*, CRC Press, Boca Raton.

[20] Press, W. H., Teukolsky, S. A., Vetterling, W. and Flannery, B. P. (2002), *Numerical Recipies in C++: the Art of Scientific Computing*, Cambridge University Press, Cambridge.

[21] Sefrioui, J. and Gosselin, C. M. (1995), 'On the quadratic nature of the singularity curves of planar three-degree-of-freedom parallel manipulators', *Mechanism and Machine Theory*, **30**, pp. 533–551.

[22] St-Onge, B. M. and Gosselin, C. (1996), 'Singularity analysis and representation of spatial six-dof parallel manipulators', *Recent Advances in Robot Kinematics*, pp. 389–398.

[23] St-Onge, B. M. and Gosselin, C. (2000), 'Singularity analysis and representation of the general Gough-Stewart platform', *International Journal of Robotics Research*, **19**(3), pp. 271–288.

[24] Wolfram, S. (2004), *The Mathematica Book*, Cambridge University Press, Cambridge.

A Different parameterizations of $SO(3)$

In this section, we discuss the parameterizations of $SO(3)$ used in this paper.

A.1 Rodrigue's parameters

Rodrigue's parameters utilizes the isomorphism between $\Re^3$ and $so(3)$, and provide an algebraic parameterization of $SO(3)$ (see, for e.g., [15]). Using the isomorphism, we can obtain a 3×3 skew-symmetric matrix $\boldsymbol{A}$ corresponding to a vector $\boldsymbol{c} = (c_1, c_2, c_3)^T$ as

$$\boldsymbol{A} = \begin{pmatrix} 0 & -c_3 & c_2 \\ c_3 & 0 & -c_1 \\ -c_2 & c_1 & 0 \end{pmatrix} \tag{37}$$

There exists a homeomorphism from the neighborhood of $\mathbf{0} \in so(3)$ to a neighborhood of $\boldsymbol{I}_3 \in SO(3)$ due to Cayley, given by

$$\boldsymbol{R} = (\boldsymbol{I}_3 - \boldsymbol{A})(\boldsymbol{I}_3 + \boldsymbol{A})^{-1} \tag{38}$$

where $\boldsymbol{I}_3$ is the identity in $GL_3(\Re)$. Using this transformation, we can get one of the possible explicit formulæ for the elements of $\boldsymbol{R} \in SO(3)$ as

$$R_{ij} = \frac{1}{1 + c_k^2}((1 - c_k^2 + 2c_i^2)\delta_{ij} + 2(1 - \delta_{ij})(c_i c_j - c_k \epsilon_{ijk})) \tag{39}$$

In matrix form, we can write

$$\boldsymbol{R} = \frac{1}{1 + c_1^2 + c_2^2 + c_3^2} \begin{pmatrix} 1 + c_1^2 - c_2^2 - c_3^2 & 2(c_1c_2 - c_3) & 2(c_1c_3 + c_2) \\ 2(c_1c_2 + c_3) & 1 - c_1^2 + c_2^2 - c_3^2 & 2(c_2c_3 - c_1) \\ 2(c_1c_3 - c_2) & 2(c_2c_3 + c_1) & 1 - c_1^2 - c_2^2 + c_3^2 \end{pmatrix} \tag{40}$$

For any rotation matrix $\boldsymbol{R}$. we have $\mathrm{tr}(\boldsymbol{R}) = 1 + 2\cos\theta$, where $\theta \in [0, \pi]$ is the net rotation represented by $\boldsymbol{R}$. Hence we have

$$1 + 2\cos\theta = \mathrm{tr}(\boldsymbol{R}) = \frac{3 - c_1^2 - c_2^2 - c_3^2}{1 + c_1^2 + c_2^2 + c_3^2}$$

If $\theta \neq 0, m\pi$ where m is an integer, the rotation axis is well defined, and is given by the unit vector $\boldsymbol{u} = (u_x, u_y, u_z)$, where

$$2\sin\theta u_k = R_{ij}\epsilon_{ijk} = \frac{4c_k}{1 + c_1^2 + c_2^2 + c_3^2}$$

It can be shown that these requirements are simultaneously satisfied if we have:

$$\boldsymbol{c} = \boldsymbol{u}\tan(\theta/2) \tag{41}$$

Equation (41) gives the geometric interpretation of c_i, which are known as *Rodrigue's parameters*. These parameters provide a system of local coordinates of $SO(3)$ in the neighborhood of its identity. The major advantage of this representation of rigid-body rotation is in its algebraic nature, which makes its use in complicated kinematic analysis computationally economical.

A.2 *Ball* parameters of $SO(3)$

The geometric interpretation of c_i leads to a 4-parameter representation of $SO(3)$ in terms of (u_x, u_y, u_z, θ). However, $SO(3)$ is 3-dimensional, and this parameterization involves a constraint, i.e., $\|\boldsymbol{u}\| = 1$. One can further parameterize the unit vector $\boldsymbol{u}$ to obtain a *constraint free* parameterization of $SO(3)$ as explained below.

The unit vector parallel to the rotation axis can be written as

$$\boldsymbol{u} = (\cos\alpha\cos\beta, \cos\alpha\sin\beta, \sin\alpha)^T \tag{42}$$

where α is the angle made by $\boldsymbol{u}$ with the XY plane, and β is the angle made by the projection of $\boldsymbol{u}$ on the XY plane with the X axis. We can now express $\boldsymbol{c}$ as

$$\boldsymbol{c} = \tan(\theta/2)(\cos\alpha\cos\beta, \cos\alpha\sin\beta, \sin\alpha)^T \tag{43}$$

The three quantities (α, β, θ) form another local parameterization of $SO(3)$, and are related to the representation of $SO(3)$ as a *ball* [18]. The angles α, β serve as the latitude and longitude, while $\theta \in [0, \pi]$ gives the radius. Each point on the surface of this ball represents a rotation uniquely. However, a given rotation corresponds to two points on the ball, which are antipodal to each other. This is because the rotation $(\boldsymbol{u}, \theta)$ is equivalent to the rotation $(-\boldsymbol{u}, -\theta)$ $\forall \theta \in [0, \pi]$, and it can be shown that the ball is a *doubly connected* domain. The zero rotation corresponds to the center. Entire $SO(3)$ can be covered if the axis is swept through the unit sphere $\mathbb{S}^2$, and the magnitude of rotation varies from 0 to π for each such axis, i.e., $\alpha \in [-\pi/2, \pi/2]$, $\beta \in [0, 2\pi]$, $\theta \in [0, \pi]$. The advantage of this parameterization over more common ones, such as the Euler angles, is that it yields an intuitive idea of the top platform orientation directly. It can also take advantage of the compactness of the kinematic expressions in terms of c_i via equation (43), providing geometric insight at the same time.

View publication stats